Available online at www.sciencedirect.com
ScienceDirect
Journal of Computational Physics 224 (2007) 992–1020
JOURNAL OF COMPUTATIONAL PHYSICS
www.elsevier.com/locate/jcp

High order residual distribution conservative finite difference WENO schemes for convection–diffusion steady state problems on non-smooth meshes

Ching-Shan Chou [1], Chi-Wang Shu *

Division of Applied Mathematics, Brown University, Providence, RI 02912, United States

Received 18 May 2006; received in revised form 30 October 2006; accepted 4 November 2006
Available online 19 December 2006

Abstract

In this paper, we propose a high order residual distribution conservative finite difference scheme for solving convection–diffusion equations on non-smooth Cartesian meshes. WENO (weighted essentially non-oscillatory) integration and linear interpolation for the derivatives are used to compute the numerical fluxes based on the point values of the solution. The objective is to obtain a high order scheme which, for two space dimension, has a computational cost comparable to that of a high order WENO finite difference scheme and is therefore much lower than that of a high order WENO finite volume scheme, yet it does not have the restriction on mesh smoothness of the traditional high order conservative finite difference schemes, hence it would be more flexible for the resolution of sharp layers. The principles of residual distribution schemes are adopted to obtain steady state solutions. The distribution of residuals resulted from the convective and diffusive parts of the PDE is carefully designed to maintain the high order accuracy. The proof of a Lax-Wendroff type theorem is provided for convergence towards weak solutions in one and two dimensions under additional assumptions. Extensive numerical experiments for one and two-dimensional scalar problems and systems confirm the high order accuracy and good quality of our scheme to resolve the inner or boundary layers.

Keywords: Residual distribution; Fluctuation splitting; WENO integration; High order accuracy; Convection–diffusion equations; Steady state

1. Introduction

In this paper, we are interested in designing high order conservative finite difference schemes for steady state convection–diffusion equations

$$u_t + \nabla \cdot F(u) = \nabla \cdot (a(u,x)\nabla u), \tag{1.1}$$

* Corresponding author. Tel.: +1 401 863 2549; fax: +1 401 863 1355.
E-mail addresses: cschou@math.uci.edu (C.-S. Chou), shu@dam.brown.edu (C.-W. Shu).
[1] Present address: Department of Mathematics, University of California at Irvine, Irvine, CA 92697, United States.

0021-9991/$ - see front matter
doi:10.1016/j.jcp.2006.11.006

where $\frac{\partial F(u)}{\partial u} \cdot \xi$ is diagonalizable with real eigenvalues for any real vector ξ, and the matrix $a(u,x)$ is semi-positive definite. This type of problems is found in a wide range of applications such as the Navier–Stokes equations in gas dynamics and the hydrodynamic and energy transport models in semiconductor device simulations. The first derivatives in Eq. (1.1) are associated with convection while the second derivatives are responsible for diffusion. The solution of Eq. (1.1) is smooth where the diffusion does not vanish. It is also well known that the diffusion terms give rise to inner or boundary layers. In order to resolve the layers, local grid refinement is advantageous, and we could have abrupt changes in mesh sizes. In practice, high order conservative finite difference schemes (e.g. the WENO scheme in [12]) are favorable for multi-dimensional problems due to their lower computational cost comparing with finite volume schemes. However, they have problems handling abrupt changes in mesh sizes, and the accuracy might be lost due to the non-uniform mesh.

To overcome the aforementioned difficulties, it is desirable to develop high order conservative schemes which are of the finite difference type (the numerical approximations are the point values of the solution and on structured meshes approximations to derivatives or integrals can be performed dimension by dimension) and have a computational cost comparable to that of regular finite difference schemes, yet the meshes are allowed to be arbitrary Cartesian or curvilinear without any smoothness assumption. In this paper, our effort is restricted to steady state problems (solutions to (1.1) which are time independent). Time dependent problems are significantly more difficult and will be left for future work. The work in this paper is an extension of our previous work [8], in which we adopted the idea of ''Residual Distribution'' and developed schemes with the above properties for steady state hyperbolic conservation laws.

The class of residual distribution (RD) schemes, or fluctuation splitting schemes for solving steady state hyperbolic conservation laws

$$\nabla \cdot F(u) = 0 \tag{1.2}$$

was first introduced by Roe, Sidilkover, Deconinck, Struijs, Bourgeois et al. [20,9,22] and followed by later works in, e.g. [23,24,1,3,4,6,5,14]. The RD schemes use a pointwise representation of the solution, same as in finite difference schemes, and it allows conservative approximations with high order accuracy on very general meshes. The RD schemes are composed of two parts: residual evaluation and residual distribution. The framework of a residual distribution scheme for a two-dimensional conservation law (1.2) is given as follows. We are given a general triangular or quadrilateral mesh, with n_t elements $\{T_j\}_{j=1,\ldots,n_t}$ and n_s nodes $\{M_i\}_{i=1,\ldots,n_s}$ which are the vertices of these elements. The residual Φ^T over the element T is defined and decomposed as

$$\Phi^T = \int_T \mathrm{div} F^h(u_h)\,\mathrm{d}x, \quad \sum_{i,M_i \in T} \Phi_i^T = \Phi^T, \tag{1.3}$$

where F^h is an approximation of the flux function F in (1.2), and the total residual Φ^T over the element T is decomposed to a sum of residuals Φ_i^T to be distributed to each node M_i of T. The design principles for the distribution of the residual are described in [1]. In particular, the so-called *residual property* should hold, which states that $|\Phi_i^T|/|\Phi^T|$ should be uniformly bounded. This would imply that when the zero cell residual limit $\Phi^T = 0$ is reached, the distributed residuals Φ_i^T are also zeros. The dual cells, C_i, $i = 1, \ldots, n_s$ are obtained by joining the centroids of the elements T_j having M_i as one of the nodes, to the mid-points of the edges of T_j. If we denote the collection of elements T_j having M_i as one of the nodes as S_i, then the residual distribution scheme is given as

$$u_i^{n+1} = u_i^n - \frac{\Delta t_n}{|C_i|} \sum_{T \in S_i} \Phi_i^T. \tag{1.4}$$

At steady state, with vanishing cell residuals, the accuracy can be obtained.

To extend RD scheme to convection–diffusion equations, efforts were made to properly discretize and distribute the diffusion terms in Eq. (1.1). In [17], Paillère et al. propose two discretizations: one is to use a RD scheme for the convection terms while adding a Galerkin discretization of the diffusion terms; the other is a residual based scheme in which one has to compute the residual from the diffusion terms and distribute the

residuals from convective and diffusive parts together with the upwind coefficients. The former discretization is physically reasonable since the diffusion does not have a preferred spatial direction, and it has been applied to Navier–Stokes equations [25]. There are also works devoted to high order discretizations for the diffusion terms, e.g. [13,7,15]. In [16], Nishikawa and Roe point out that the Galerkin discretization for the diffusion terms would lead to a loss of order of accuracy, according to truncation error analysis. They propose to write the governing equations as a first order system to get high order accuracy. Using a different technique, Ricchiuto et al. [18] rewrite the RD scheme as a perturbation of the Galerkin scheme weighted by a properly scaled function, so that the scheme gives a correct behavior for the convection or diffusion dominated regimes. The scaling depends on a cell Peclet number, which in scalar linear advection–diffusion equations is defined as $\frac{h^T\sqrt{\vec{k}\cdot\vec{k}}}{v}$, where h^T is the reference length scale for cell T, $\vec{k}$ is the speed associated with the convection terms and v is the viscosity coefficient of the diffusion terms.

In the present paper, we propose high order finite difference schemes on rectangular meshes which are not necessarily smooth. The cell residuals in Eq. (1.3) are modified to be

$$\Phi^T = \int_T \mathrm{div} F^h(u_h)\,\mathrm{d}x - \int_T \nabla\cdot(a(u,x)\nabla u)\,\mathrm{d}x. \tag{1.5}$$

We evaluate the cell residuals through WENO integration with the first derivatives interpolated by central difference. The main purpose of this restriction on the meshes is the observation that the evaluation of the residuals in Eq. (1.5) in 2D, which is in general two-dimensional integrals, can be decomposed to a dimension by dimension one-dimensional computation. This is the key to save the computational costs. As for residual distribution, the distribution coefficients are no long purely upwind, but weighted by a cell Peclet number defined above, which measures the relative importance of the convection terms with respect to the diffusion terms.

This paper is organized as follows. In Sections 2 and 3, we describe the residual evaluation and the residual distribution procedures for one and two-dimensional problems respectively. Section 4 contains extensive numerical simulation results for one and two-dimensional scalar and system steady state problems to demonstrate the good behavior of our scheme. Concluding remarks are given in Section 5. The Lax-Wendroff type theorem for convergence towards weak solutions is proven for the one-dimensional case in Section 2 and for the two-dimensional case in Appendix.

2. High order RD finite difference WENO schemes in one dimension

In this section, we design a residual distribution finite difference WENO scheme for one-dimensional steady state convection–diffusion equations. In the first subsection, we define the residual through integral form, and then describe the distribution of residuals. The distribution is designed through a cell Peclet number and follows the principles of the residual property. In the second subsection, we generalize the scheme to one-dimensional systems, based on a local characteristic field decomposition, and distribute the residuals as in the scalar case in the characteristic fields.

2.1. One-dimensional scalar problems

We have the one-dimensional scalar steady state problem

$$f(u)_x = g(u,x) + vu_{xx}, \quad v \geqslant 0. \tag{2.1}$$

We define the grid to be $\{x_i\}_{i=0,\ldots,N}$, grid function $\{u_i\}_{i=0,\ldots,N}$, the interval $I_{i+\frac{1}{2}} = [x_i, x_{i+1}]$ with length $\Delta x_{i+\frac{1}{2}}$, the control volume centered at x_i to be C_i (from the mid-point of the interval $I_{i-\frac{1}{2}}$ to the mid-point of the interval $I_{i+\frac{1}{2}}$), and the length of C_i is denoted by $|C_i|$.

The residual in the interval $I_{i+\frac{1}{2}}$ is define by

$$\Phi_{i+\frac{1}{2}} = \int_{x_i}^{x_{i+1}} (f(u)_x - g(u,x) - vu_{xx})\,\mathrm{d}x = f(u_{i+1}) - f(u_i) - \int_{x_i}^{x_{i+1}} g(u,x)\,\mathrm{d}x - vu_x(x_{i+1}) + vu_x(x_i). \tag{2.2}$$

If we can reach the zero cell residual limit, i.e. if $\Phi_{i+\frac{1}{2}} = 0$ for all i, then the accuracy of the scheme is determined by the accuracy of the approximation to $\int_{x_i}^{x_{i+1}} g(u,x)\,dx$, $u_x(x_i)$ and $u_x(x_{i+1})$. In our scheme, we use a fourth order central WENO integration, which is described in [8], to approximate the integral $\int_{x_i}^{x_{i+1}} g(u,x)\,dx$. To approximate the derivatives associated with the diffusion term, for example $u_x(x_i)$, we use the central stencil $\{x_{i-2}, x_{i-1}, x_i, x_{i+1}, x_{i+2}\}$, and express the approximation as a linear combination of the point values in the stencil, namely,

$$u_x(x_i) = \sum_{m=-2}^{2} c_i^m u_{i+m} + O(\Delta x^4), \tag{2.3}$$

where c_i^m depends on the mesh sizes in the stencil and can be pre-computed once given the grid. Fourth order accuracy is therefore guaranteed at the zero cell residual limit. We remark that the first derivatives are evaluated to form the residual of the diffusion terms u_{xx} in Eq. (2.1), which is dissipative in nature, and hence it is reasonable to use linear weights in Eq. (2.3). Our numerical experience reveals that using linear weights rather than WENO weights in (2.3) is crucial in getting correct solutions. As an extreme example, if the initial condition is a discontinuous step function, then a WENO approximation of the derivative u_x is almost zero everywhere, since the stencil which crosses the discontinuity has a very small weight. This would imply that the viscous terms in the residual (2.2) give almost zero contribution even for the cell crossing the discontinuity, which is clearly incorrect.

Next, we start to distribute the residuals. We note that the residual is composed of two parts. One is from the convection term, which we denote by $\Phi^c_{i+\frac{1}{2}}$

$$\Phi^c_{i+\frac{1}{2}} = f(u_{i+1}) - f(u_i) - \int_{x_i}^{x_{i+1}} g(u,x)\,dx, \tag{2.4}$$

and the other part is from the diffusion term, denoted by $\Phi^d_{i+\frac{1}{2}}$

$$\Phi^d_{i+\frac{1}{2}} = -\nu u_x(x_{i+1}) + \nu u_x(x_i). \tag{2.5}$$

By the nature of convection, upwinding is needed to distribute $\Phi^c_{i+\frac{1}{2}}$, as described in [1]. As for the residual $\Phi^d_{i+\frac{1}{2}}$ associated with diffusion, isotropic distribution is more appropriate since there is no preferred spatial direction for the diffusive part. In [16], the authors pointed out that if we distribute $\Phi^c_{i+\frac{1}{2}}$ and $\Phi^d_{i+\frac{1}{2}}$ separately, the order of accuracy would be compromised and this can be expected through truncation error analysis. Numerical experiments also reveal the degrading to first order accuracy due to the incompatible distribution. Therefore, to maintain high order accuracy, we should distribute $\Phi^c_{i+\frac{1}{2}}$ and $\Phi^d_{i+\frac{1}{2}}$ altogether, namely, distribute $\Phi_{i+\frac{1}{2}}$, and meanwhile recognize the dominating effect in the cell. In this paper, we follow a type of distribution proposed in [16]. The details are explained as follows.

In the interval $[x_i, x_{i+1}]$, the residual is $\Phi_{i+\frac{1}{2}}$, and it is to be distributed to the nodes x_i and x_{i+1}. For simplicity and with no ambiguity, we drop the subscript $i+\frac{1}{2}$ for the residuals. Here we denote the residual distributed to the point x_{i+1} and x_i as Φ^+ and Φ^- respectively. We require $\Phi = \Phi^+ + \Phi^-$ for the conservation and require $|\Phi^\pm|/|\Phi|$ to be uniformly bounded by the residual property [1], which implies that when the zero cell residual limit $\Phi_{i+\frac{1}{2}} = 0$ is reached, the distributed residuals $\Phi^\pm$ are also zeros. Inspired by [16], one way to distribute the residual is the following:

$$\Phi^+ = \hat{\alpha}\Phi, \quad \Phi^- = (1-\hat{\alpha})\Phi, \quad \hat{\alpha} \in [0,1] \tag{2.6}$$

with the distribution coefficient $\hat{\alpha}$ defined by

$$\hat{\alpha} = \frac{\alpha + \frac{k\nu}{2(|\bar{\lambda}|+\epsilon)\Delta x_{i+\frac{1}{2}}}}{1 + \frac{k\nu}{(|\bar{\lambda}|+\epsilon)\Delta x_{i+\frac{1}{2}}}}. \tag{2.7}$$

In Eq. (2.7), $\bar{\lambda} = (f'(\bar{u}), \bar{u})$ is the average state in the cell taken to be $\frac{1}{2}(u_i + u_{i+1})$, k is chosen accordingly in the problem, ϵ is a small number which avoids the denominator to be zero and is taken as 10^{-6} in our tests. The number α is the distribution coefficient associated with the convection and is determined by

$$\alpha = \begin{cases} 1, & \text{if } \bar{\lambda} \geqslant \varepsilon, \\ 0, & \text{if } \bar{\lambda} \leqslant -\varepsilon, \\ r(\bar{\lambda}, \varepsilon), & \text{otherwise}, \end{cases}$$

where $\bar{\lambda}$ is defined as above. The function $r(\cdot,\cdot)$ is the entropy correction function for the Roe scheme [10] defined by

$$r(\lambda, \varepsilon) = \frac{1}{4\varepsilon^3}(\lambda + \varepsilon)^2(2\varepsilon - \lambda) \tag{2.8}$$

and ε is chosen accordingly in the problem.

From Eq. (2.7), we note that if the diffusion is very small relatively in a cell, the distribution coefficient $\hat{\alpha}$ is close to α, so upwinding plays the role in the distribution. Conversely, if the diffusion dominates, $\hat{\alpha}$ is close to $\frac{1}{2}$, and isotropic distribution takes place in the cell.

Finally, the point value u_i is updated through sending the distributed residuals to the point x_i, as in a pseudo time-marching scheme, which can be written as a semi-discrete system

$$\frac{\mathrm{d}u_i}{\mathrm{d}t} + \frac{1}{|C_i|}(\Phi^+_{i-\frac{1}{2}} + \Phi^-_{i+\frac{1}{2}}) = 0. \tag{2.9}$$

In our numerical experiments, we use a third order TVD Runge–Kutta scheme [21] for the (pseudo) time discretization. Since the accuracy in time is irrelevant here, any stable time marching can be used, and strategies such as preconditioning and multigrid can be used to accelerate convergence towards steady state, but we do not pursue these approaches in this paper. Because of the residual property, namely the uniform boundedness of $|\Phi^{\pm}|/|\Phi|$, a zero cell residual limit $\Phi_{i+\frac{1}{2}} = 0$ is clearly also a steady state solution of (2.9). Conversely, a steady state solution of (2.9) may not imply a zero cell residual limit $\Phi_{i+\frac{1}{2}} = 0$ for all i. In fact, a simple counting of the number of unknowns and the number of cell-residuals would show an over-determined system if the solution at both boundaries are prescribed, hence it may not be realistic to always require a zero cell residual. Our numerical experiments indicate that, near shocks or sharp gradients, $\Phi_{i+\frac{1}{2}}$ may not be small even if the steady state solution of (2.9) is reached. Convergence towards weak solutions in this case would thus need to rely on a Lax-Wendroff type theorem stated and proved in the following. We remark here that in the proof, due to some technical difficulties, we additionally assume that the mesh is uniform or smoothly varying. This assumption does not seem necessary according to our numerical experiments, and we are still exploring a proof for non-smooth meshes. Most of the numerical results presented in this paper are performed on non-smooth meshes.

As defined in Eq. (2.2), (2.4) and (2.5), the residual is defined by

$$\Phi_{i+\frac{1}{2}} = \Phi^{\mathrm{c}}_{i+\frac{1}{2}} + \Phi^{\mathrm{d}}_{i+\frac{1}{2}},$$

where the convective and diffusive residuals are given by

$$\begin{aligned} \Phi^{\mathrm{c}}_{i+\frac{1}{2}} &= f(u_{i+1}) - f(u_i) - \mathscr{R}(g(u_{\Delta x}, x), I_{i+\frac{1}{2}}) \\ \Phi^{\mathrm{d}}_{i+\frac{1}{2}} &= -\nu\mathscr{D}(u_{\Delta x}, x_{i+1}) + \nu\mathscr{D}(u_{\Delta x}, x_i), \end{aligned} \tag{2.10}$$

where $\mathscr{R}(g(u_{\Delta x}, x), I_{i+\frac{1}{2}})$ is an approximation of $\int_{I_{i+\frac{1}{2}}} g(u, x)\,\mathrm{d}x$, which can be written as a linear combination of the point values of g. The quantity $\mathscr{D}(u_{\Delta x}, x_i)$ approximates $u_x(x_i)$ and can be written as a linear combination of the point values of u,

$$\mathscr{D}(u_{\Delta x}, x_i) = \sum_{k=-r+1}^{r-1} c_i^k u_{i+k}. \tag{2.11}$$

which is of $(2r-2)$th order accuracy. Since we use symmetric linear weights to approximate the derivatives, and furthermore (for the proof of the Lax-Wendroff type theorem) assume the mesh is uniform, we have

$$c_i^k = c^k, \quad c^k = -c^{-k}. \tag{2.12}$$

The distributed residuals, as defined in Eq. (2.6), are $\Phi^{\pm}_{i+\frac{1}{2}}$, with the conservation property,

$$\Phi_{i+\frac{1}{2}} = \Phi^{+}_{i+\frac{1}{2}} + \Phi^{-}_{i+\frac{1}{2}} \tag{2.13}$$

and the residual property

$$\frac{|\Phi^{\pm}_{i+\frac{1}{2}}|}{|\Phi_{i+\frac{1}{2}}|} \leqslant C, \tag{2.14}$$

where here and below C with or without subscriptions denotes constants independent of the mesh sizes. Equipped with the above properties, we have the following Lax-Wendroff type theorem.

Theorem 2.1. *Assume that the flux function f in Eq. (2.1) is Lipschitz continuous, and the source term $g(u,x)$ is continuous in both arguments. Suppose that the mesh is uniform: $\Delta x_{i+\frac{1}{2}} = \Delta x$. If $u_{\Delta x}$ is a steady state solution of Eq. (2.9) satisfying Eqs. (2.10), (2.13) and (2.14), and if there is a function u with bounded total variation such that*

$$u_{\Delta x} \to u \quad \text{in } L^1(\mathbb{R}), \quad \text{as } \Delta x \to 0$$

and

$$\sup_{\Delta x} \sup_{x} |u_{\Delta x}(x)| \leqslant C_1$$

then u is a weak solution to Eq. (2.1).

Proof. At steady state of the scheme, $\Phi^{+}_{i-\frac{1}{2}} + \Phi^{-}_{i+\frac{1}{2}} = 0$ for all i. Let $\varphi \in C^{\infty}_0(\mathbb{R})$ be a test function, and denote $\varphi_i = \varphi(x_i)$. We have,

$$0 = \sum_i (\Phi^{+}_{i-\frac{1}{2}} + \Phi^{-}_{i+\frac{1}{2}})\varphi_i = \sum_i \Phi_{i-\frac{1}{2}}\ \varphi_i - \sum_i \Phi^{-}_{i-\frac{1}{2}}(\varphi_i - \varphi_{i-1}) = \mathrm{I} + \mathrm{II}.$$

We look at the first summation term

$$\begin{aligned}\mathrm{I} &= \sum_i \Phi_{i-\frac{1}{2}}\ \varphi_i = \sum_i (f(u_i) - f(u_{i-1}) - \mathscr{R}(g(u_{\Delta x}, x), I_{i-\frac{1}{2}}))\varphi_i - \nu \sum_i (\mathscr{D}(u_{\Delta x}, x_i) - \mathscr{D}(u_{\Delta x}, x_{i-1}))\varphi_i \\ &= -\sum_i f(u_i)\frac{(\varphi_{i+1} - \varphi_i)}{\Delta x}\Delta x - \sum_i \mathscr{R}(g(u_{\Delta x}, x), I_{i-\frac{1}{2}})\varphi_i - \nu \sum_i (\mathscr{D}(u_{\Delta x}, x_i) - \mathscr{D}(u_{\Delta x}, x_{i-1}))\varphi_i.\end{aligned}$$

Note that

$$-\sum_i f(u_i)\frac{(\varphi_{i+1} - \varphi_i)}{\Delta x}\Delta x \to -\int f(u)\varphi_x \,\mathrm{d}x, \quad \text{as } \Delta x \to 0$$

and

$$\sum_i \mathscr{R}(g(u_{\Delta x}, x), I_{i-\frac{1}{2}})\varphi_i \to \int g(u,x)\varphi \,\mathrm{d}x, \quad \text{as } \Delta x \to 0.$$

Moreover, equipped with Eqs. (2.11) and (2.12), we have

$$\begin{aligned}\sum_i (\mathscr{D}(u_{\Delta x}, x_i) - \mathscr{D}(u_{\Delta x}, x_{i-1}))\varphi_i &= \sum_i \mathscr{D}(u_{\Delta x}, x_i)(\varphi_i - \varphi_{i+1}) = \sum_i \sum_{k=-r+1}^{r-1} c^k u_{i+k}(\varphi_i - \varphi_{i+1}) \\ &= \sum_i u_i \sum_{k=-r+1}^{r-1} c^k(\varphi_{i-k} - \varphi_{i-k+1}) = \sum_i u_i \sum_{k=-r+1}^{r-1} -c^{-k}(\varphi_{i-k} - \varphi_{i-k+1}) \\ &= \sum_i u_i \sum_{k=-r+1}^{r-1} c^k(\varphi_{i+1+k} - \varphi_{i+k}) = \sum_i u_i \frac{\mathscr{D}(\varphi(x), x_{i+1}) - \mathscr{D}(\varphi(x), x_i)}{\Delta x}\Delta x.\end{aligned}$$

Therefore,

$$\sum_i (\mathscr{D}(u_{\Delta x}, x_i) - \mathscr{D}(u_{\Delta x}, x_{i-1}))\varphi_i \to \int u\varphi_{xx}\,\mathrm{d}x, \quad \text{as } \Delta x \to 0$$

and

$$\mathrm{I} \to -\int f(u)\ \varphi_x\,\mathrm{d}x - \int g(u,x)\ \varphi\,\mathrm{d}x - \nu\int u\varphi_{xx}\,\mathrm{d}x.$$

Next, we estimate the second term II

$$\begin{aligned}
|\mathrm{II}| &= \left|\sum_i \Phi^-_{i-\frac{1}{2}}(\varphi_i - \varphi_{i-1})\right| \leqslant \sum_i |\Phi^-_{i-\frac{1}{2}}||\varphi_i - \varphi_{i-1}| \leqslant C\sum_i |\Phi_{i-\frac{1}{2}}||\varphi_i - \varphi_{i-1}| \\
&\leqslant C\sum_i |f(u_i) - f(u_{i-1})||\varphi_i - \varphi_{i-1}| + C\sum_i |\mathscr{R}(g(u_{\Delta x}, x), I_{i-\frac{1}{2}})|\frac{|\varphi_i - \varphi_{i-1}|}{\Delta x}\Delta x + \nu\sum_i |\mathscr{D}(u_{\Delta x}, x_i) \\
&\quad - \mathscr{D}(u_{\Delta x}, x_{i-1})||\varphi_i - \varphi_{i-1}| \\
&\leqslant C_2\sum_i |u_i - u_{i-1}|\Delta x + C_2\Delta x\sum_i |\mathscr{R}(g(u_{\Delta x}, x), I_{i-\frac{1}{2}})|\frac{|\varphi_i - \varphi_{i-1}|}{\Delta x}.
\end{aligned}$$

The second term above without the Δx factor converges to $C_2\int |g(u,x)\varphi_x|\,\mathrm{d}x$ and hence the second term itself is $O(\Delta x)$. As for the first term,

$$\sum_i |u_i - u_{i-1}|\Delta x \leqslant \sum_i |u_i - u(x_i)|\Delta x + \sum_i |u(x_i) - u(x_{i-1})|\Delta x + \sum_i |u(x_{i-1}) - u_{i-1}|\Delta x.$$

By the L^1 convergence of the scheme and the fact that $u(x)$ has bounded total variation, $|\mathrm{II}| \to 0$ as $\Delta x \to 0$, and we can conclude that

$$-\int f(u)\ \varphi_x\,\mathrm{d}x - \int g(u,x)\ \varphi\,\mathrm{d}x - \nu\int u\varphi_{xx}\,\mathrm{d}x = 0$$

namely, u is a weak solution to Eq. (2.1). □

We now summarize the procedure of the high order RD finite difference WENO scheme for one-dimensional scalar problems:

1. Compute the residuals defined in Eq. (2.2) using WENO integration and linear interpolation for the derivatives with a proper accuracy.
2. Distribute the residuals according to Eq. (2.6).
3. Update the point values through sending the residuals and forward in pseudo time (2.9) by a TVD Runge–Kutta time discretization until the steady state is reached.

2.2. One-dimensional systems

Consider a one-dimensional steady state system (2.1) where u, $f(u)$ and $g(u)$ are vector-valued functions in $\mathbb{R}^m$ and ν is a semi-positive definite matrix. For convection–diffusion systems, we assume that the Jacobian $f'(u)$ can be written as $L\Lambda R$, where Λ is a diagonal matrix with real eigenvalues on the diagonal, and L and R are matrices of left and right eigenvectors of $f'(u)$ respectively.

The grid, the grid function and the control volumes are denoted as in Section 2.1. The residual in the interval $[x_i, x_{i+1}]$ is again defined by Eq. (2.2). As before, the accuracy of the scheme is determined by the accuracy of the approximation to $\int_{x_i}^{x_{i+1}} g(u,x)\,\mathrm{d}x$, $u_x(x_i)$ and $u_x(x_{i+1})$. The approximated integral is obtained by a fourth order central WENO integration and the approximated derivatives are obtained by fourth order central linear interpolation given in Eq. (2.3).

In order to distribute the residual $\Phi_{i+\frac{1}{2}}$, we use a local characteristic decomposition in the interval $[x_i, x_{i+1}]$. First, we compute an average state $\bar{u}$ between u_i and u_{i+1}, using either the simple arithmetic mean or a Roe's average [19], and denote $\bar{L}$ and $\bar{R}$ to be the matrices with left and right eigenvectors L and R evaluated at the

average state, and $\bar{\lambda}_k$ the corresponding kth eigenvalue. In the following, for simplicity of the notation and with no ambiguity, we drop the subscript $i+\frac{1}{2}$ in the residuals. We project the residual Φ to the characteristic fields, namely, $\Psi = \bar{R}\Phi$. The residual Ψ is to be distributed to the two endpoints x_i and x_{i+1}, and we denote the residual sent to x_{i+1} and x_i by Ψ^+ and Ψ^-, respectively, with $\Psi = \Psi^+ + \Psi^-$. Those residuals are defined by

$$\Psi^+ = \Sigma\Psi, \quad \Psi^- = (I - \Sigma)\Psi, \tag{2.15}$$

where I is the identity matrix and Σ is a diagonal matrix with the mth diagonal component

$$\Sigma_{mm} = \frac{\alpha_m + \frac{k|v|}{2(|\bar{\lambda}_m|+\epsilon)\Delta x_{i+\frac{1}{2}}}}{1 + \frac{k|v|}{(|\bar{\lambda}_m|+\epsilon)\Delta x_{i+\frac{1}{2}}}} \tag{2.16}$$

with ϵ taken as 10^{-6} to avoid the denominator to be zero, and $|v|$ the spectral radius of the matrix v. The number α_m is the distribution coefficient associated with convection in mth characteristic field

$$\alpha_m = \begin{cases} 1, & \text{if } \bar{\lambda}_m \geqslant \varepsilon, \\ 0, & \text{if } \bar{\lambda}_m \leqslant -\varepsilon, \\ r(\bar{\lambda}_m, \varepsilon), & \text{otherwise}, \end{cases}$$

with the function $r(\cdot,\cdot)$ defined in Eq. (2.8) and ε chosen accordingly in the problem.

Next, we project the distributed residuals back to the physical space, and denote Φ^+ and Φ^- to be the residuals in the physical space which are sent to the points x_{i+1} and x_i, respectively

$$\Phi^+ = \bar{L}\Psi^+, \qquad \Phi^- = \bar{L}\Psi^-. \tag{2.17}$$

Finally, as in the scalar case, the point value u_i can be updated in the pseudo time-marching semi-discrete scheme (2.9), which is again discretized by a third order TVD Runge–Kutta scheme in our numerical experiments until the steady state is reached.

We now summarize the procedure of the high order RD finite difference WENO scheme for one-dimensional steady state systems:

1. Compute the residuals defined in Eq. (2.2) using WENO integration and linear interpolation for the derivatives with a proper accuracy.
2. Project the residuals to local characteristic fields.
3. Distribute the residuals with coefficients defined in Eq. (2.15) in the characteristic fields.
4. Project the distributed residuals in characteristic fields back to the physical space as in (2.17).
5. Update the point values through sending the residuals in the physical space and forward in pseudo time (2.9) by a TVD Runge–Kutta time discretization until the steady state is reached.

3. High order RD finite difference WENO schemes in two dimension

In this section, we design a high order RD finite difference WENO scheme for two-dimensional steady state convection–diffusion problems on non-smooth curvilinear meshes. To be precise, we restrict our attention to such curvilinear meshes which can be smoothly mapped to non-smooth Cartesian meshes. We would then solve a modified PDE on a (non-smooth) Cartesian mesh. We therefore only need to describe our algorithm for Cartesian meshes. In Section 3.1, we define the residuals from the integral form, as in Eq. (1.5), and then describe the distribution mechanism. In Section 3.2, we extend the scheme to two-dimensional systems, based on a local characteristic field decomposition, and distribute the residuals in characteristic fields dimension by dimension.

3.1. Two-dimensional scalar problems

We have the two-dimensional scalar steady state problem

$$f(u)_x + g(u)_y = h(u,x,y) + v(u_{xx} + u_{yy}) \quad v \geqslant 0. \tag{3.1}$$

We define the grid to be $\{(x_i, y_j)\}$, grid function $\{u_{ij}\}$, the cells $I_{i+\frac{1}{2},j+\frac{1}{2}} = [x_i, x_{i+1}] \times [y_j, y_{j+1}]$, the control volume centered at (x_i, y_j) to be C_{ij} (formed by connecting the centers of the four cells sharing (x_i, y_j) as a common node), and the area of C_{ij} is denoted by $|C_{ij}|$. We also denote $\Delta x_{i+\frac{1}{2}} = x_{i+1} - x_i$ and $\Delta y_{j+\frac{1}{2}} = y_{j+1} - y_j$.

The residual in the cell $I_{i+\frac{1}{2},j+\frac{1}{2}}$ is defined by

$$\begin{aligned}
\Phi_{i+\frac{1}{2},j+\frac{1}{2}} &= \int_{y_j}^{y_{j+1}} \int_{x_i}^{x_{i+1}} (f(u)_x + g(u)_y - h(u,x,y) - v(u_{xx} + u_{yy}))\,\mathrm{d}x\,\mathrm{d}y \\
&= \int_{y_j}^{y_{j+1}} (f(u(x_{i+1},y)) - f(u(x_i,y)))\,\mathrm{d}y + \int_{x_i}^{x_{i+1}} (g(u(x,y_{j+1})) - g(u(x,y_j)))\,\mathrm{d}x \\
&\quad - \int_{y_j}^{y_{j+1}} \int_{x_i}^{x_{i+1}} h(u(x,y),x,y)\,\mathrm{d}x\,\mathrm{d}y - \int_{y_j}^{y_{j+1}} v(u_x(x_{i+1},y) - u_x(x_i,y))\,\mathrm{d}y \\
&\quad - \int_{x_i}^{x_{i+1}} v(u_y(x,y_{j+1}) - u_y(x,y_j))\,\mathrm{d}x. \qquad (3.2)
\end{aligned}$$

If we reach the zero cell residual limit, i.e. if $\Phi_{i+\frac{1}{2},j+\frac{1}{2}} = 0$ for all i and j, the accuracy of the scheme is determined by the accuracy of the approximations to the derivatives and the integrations. The approximations of the derivatives $u_x(\cdot,\cdot)$ and $u_y(\cdot,\cdot)$ are obtained from one-dimensional fourth order central linear interpolation given in Eq. (2.3).

To approximate the integration of the fluxes and the derivatives, which are one-dimensional integrals, we use a fourth order central WENO integration. As for the source term $\int_{y_j}^{y_{j+1}} \int_{x_i}^{x_{i+1}} h(u,x,y)\,\mathrm{d}x\,\mathrm{d}y$, we can approximate it in a dimension by dimension fashion, which is explained as follows. First, we define

$$H_{j+\frac{1}{2}}(x) = \int_{y_j}^{y_{j+1}} h(u(x,y),x,y)\,\mathrm{d}y$$

and hence

$$\int_{y_j}^{y_{j+1}} \int_{x_i}^{x_{i+1}} h(u,x,y)\,\mathrm{d}x\,\mathrm{d}y = \int_{x_i}^{x_{i+1}} H_{j+\frac{1}{2}}(x)\,\mathrm{d}x.$$

The integral $\int_{x_i}^{x_{i+1}} H_{j+\frac{1}{2}}(x)\,\mathrm{d}x$ can be approximated by a fourth order WENO integration in the x-direction, using $\{H_{j+\frac{1}{2}}(x_{i+k})\}_{k=-1,\ldots,2}$. By the definition of $H_{j+\frac{1}{2}}(x)$, $H_{j+\frac{1}{2}}(x_{i+k})$ can again be approximated by a fourth order WENO integration in the y-direction, using $\{h(u_{i+k,j+l}, x_{i+k}, y_{j+l})\}_{l=-1,\ldots,2}$. Therefore, the integration of the source term can be approximated dimension by dimension, and the fourth order accuracy is obtained at the zero cell residual limit.

Next, we start to distribute the residuals. In the cell $I_{i+\frac{1}{2},j+\frac{1}{2}} = [x_i, x_{i+1}] \times [y_j, y_{j+1}]$, the residual is $\Phi_{i+\frac{1}{2},j+\frac{1}{2}}$, and it is to be distributed to the vertices of the cell, which are defined to be $M_1 = (x_{i+1}, y_{j+1})$, $M_2 = (x_{i+1}, y_j)$, $M_3 = (x_i, y_{j+1})$ and $M_4 = (x_i, y_j)$. Here we define the residuals sent to the vertices M_l as $\Phi^l_{i+\frac{1}{2},j+\frac{1}{2}}$ for $l = 1, \ldots, 4$. For simplicity and without ambiguity, we drop the subscript $(i+\frac{1}{2}, j+\frac{1}{2})$ in the notations. For conservation and the residual property, we require $\Phi = \sum_{l=1}^{4} \Phi^l$ and $|\Phi^l|/|\Phi|$ to be uniformly bounded.

Following the one-dimensional case, one way to distribute the residual is defined by

$$\Phi^1 = \hat{\alpha}\hat{\beta}\Phi, \quad \Phi^2 = \hat{\alpha}(1-\hat{\beta})\Phi, \quad \Phi^3 = (1-\hat{\alpha})\hat{\beta}\Phi, \quad \Phi^4 = (1-\hat{\alpha})(1-\hat{\beta})\Phi, \quad \hat{\alpha}, \hat{\beta} \in [0,1]. \qquad (3.3)$$

The distribution coefficient $\hat{\alpha}$ in x-direction is given by

$$\hat{\alpha} = \frac{\alpha + \frac{kv}{2(|\bar{\lambda}_x| + \epsilon)\Delta x_{i+\frac{1}{2}}}}{1 + \frac{kv}{(|\bar{\lambda}_x| + \epsilon)\Delta x_{i+\frac{1}{2}}}}. \qquad (3.4)$$

In Eq. (3.4), $\bar{\lambda}_x = f'(\bar{u})$, $\bar{u}$ is the average state in the cell taken to be $\frac{1}{4}(u_{i,j} + u_{i+1,j} + u_{i+1,j+1} + u_{i,j+1})$, k is chosen accordingly in the problem, ϵ is a small number which avoids the denominator to be zero and is taken as 10^{-6}

in our tests. The number α is the distribution coefficient associated with the convection in the x-direction and is determined by

$$\alpha = \begin{cases} 1, & \text{if } \bar{\lambda}_x \geqslant \varepsilon, \\ 0, & \text{if } \bar{\lambda}_x \leqslant -\varepsilon, \\ r(\bar{\lambda}_x, \varepsilon), & \text{otherwise}, \end{cases}$$

where $\bar{\lambda}_x$ is defined as above and ε is chosen accordingly in the problem. The function $r(\cdot,\cdot)$ is given in Eq. (2.8).

Similarly, the distribution coefficient $\hat{\beta}$ in the y-direction is given by

$$\hat{\beta} = \frac{\beta + \frac{kv}{2(|\bar{\lambda}_y|+\epsilon)\Delta y_{j+\frac{1}{2}}}}{1 + \frac{kv}{(|\bar{\lambda}_y|+\epsilon)\Delta y_{j+\frac{1}{2}}}} \tag{3.5}$$

with $\bar{\lambda}_y = g'(\bar{u})$. The number β is the distribution coefficient associated with the convection in the y-direction and is determined by

$$\beta = \begin{cases} 1, & \text{if } \bar{\lambda}_y \geqslant \varepsilon, \\ 0, & \text{if } \bar{\lambda}_y \leqslant -\varepsilon, \\ r(\bar{\lambda}_y, \varepsilon), & \text{otherwise}. \end{cases}$$

Our numerical experience indicates that when the initial condition has shocks or sharp gradients present in the converging process, or the physical viscosity is very small, extra dissipation might be needed near those regions for the pseudo time marching towards steady state to proceed in a stable fashion. We therefore add an additional dissipation residual Φ^k_{diss} to each of Φ^k, only around regions with sharp gradients. The adding of dissipation residual is acceptable only if it is much smaller than the residual of physical viscosity. Hence, we concentrate on the cases where dissipation residuals are negligible comparing with the residuals of physical viscosity.

The dissipation residuals are defined as the following:

$$\begin{aligned}
\Phi^1_{\text{diss}} &= \frac{\delta}{2}\Delta^3\left(\frac{u_{i+1,j+1}-u_{i,j+1}}{\Delta x_{i+\frac{1}{2}}} + \frac{u_{i+1,j+1}-u_{i+1,j}}{\Delta y_{j+\frac{1}{2}}}\right), \\
\Phi^2_{\text{diss}} &= \frac{\delta}{2}\Delta^3\left(\frac{u_{i+1,j}-u_{i,j}}{\Delta x_{i+\frac{1}{2}}} + \frac{u_{i+1,j}-u_{i+1,j+1}}{\Delta y_{j+\frac{1}{2}}}\right), \\
\Phi^3_{\text{diss}} &= \frac{\delta}{2}\Delta^3\left(\frac{u_{i,j+1}-u_{i+1,j+1}}{\Delta x_{i+\frac{1}{2}}} + \frac{u_{i,j+1}-u_{i,j}}{\Delta y_{j+\frac{1}{2}}}\right), \\
\Phi^4_{\text{diss}} &= \frac{\delta}{2}\Delta^3\left(\frac{u_{i,j}-u_{i+1,j}}{\Delta x_{i+\frac{1}{2}}} + \frac{u_{i,j}-u_{i,j+1}}{\Delta y_{j+\frac{1}{2}}}\right),
\end{aligned} \tag{3.6}$$

where $\Delta = \max(\Delta x_{i+\frac{1}{2}}, \Delta y_{j+\frac{1}{2}})$ and the dissipation coefficient δ is chosen accordingly in the problem.

Finally, we define the distributed residuals by $\tilde{\Phi}^l = \Phi^l + \theta\Phi^l_{\text{diss}}$, $l = 1, \ldots, 4$, where θ is a discontinuity indicator defined by $\theta = \max(\theta_x, \theta_y)$, with the one-dimensional discontinuity indicators θ_x and θ_y for the x and y directions given as in [26]; θ_x is defined by $\theta_x = \frac{\beta}{\beta+\gamma}$ with

$$\alpha_i = |u_{i-1,j} - u_{i,j}|^2 + \varepsilon, \quad \beta = \left(\frac{\alpha_i}{\alpha_{i-1}} + \frac{\alpha_{i+1}}{\alpha_{i+2}}\right)^2, \quad \gamma = \frac{|u_{\max} - u_{\min}|^2}{\alpha_i}, \tag{3.7}$$

where $u_{\max}$ and $u_{\min}$ are the maximum and minimum values of u_{ij} for all grid points, and θ_y is defined similarly, but in the y-direction. A similar indicator with a wider stencil

$$\beta = \left(\frac{\alpha_{i-2}}{\alpha_{i-3}} + \frac{\alpha_{i-1}}{\alpha_{i-2}} + \frac{\alpha_i}{\alpha_{i-1}} + \frac{\alpha_{i+1}}{\alpha_{i+2}} + \frac{\alpha_{i+2}}{\alpha_{i+3}} + \frac{\alpha_{i+3}}{\alpha_{i+4}}\right)^2, \quad \gamma = \frac{|u_{\max} - u_{\min}|^2}{\alpha_{i-1} + \alpha_i + \alpha_{i+1} + \alpha_{i+2}}$$

with the same α_i as that defined in (3.7), is used for two-dimensional systems. Here ε is a small positive number taken as 10^{-6} in our numerical experiments. Clearly, $0 \leqslant \theta \leqslant 1$. Near a strong discontinuity, $\gamma \ll \beta$, θ is close to 1. However, in smooth regions, $\theta = O(\Delta^2)$, hence fourth order accuracy is maintained in smooth regions. This dissipation mechanism works well for our numerical experiments, but it may not be the optimal approach as it has an adjustable coefficient δ, whose choice for optimal performance seems to be problem dependent. Other dissipation mechanisms, such as the one adopted by Abgrall in [2], will be explored in the future.

The point value u_{ij} is then updated through sending the distributed residuals to the point (x_i, y_j), as in a pseudo time-marching scheme, which can be written as a semi-discrete system

$$\frac{du_{ij}}{dt} + \frac{1}{|C_{ij}|}\left(\tilde{\Phi}^4_{i+\frac{1}{2},j+\frac{1}{2}} + \tilde{\Phi}^3_{i+\frac{1}{2},j-\frac{1}{2}} + \tilde{\Phi}^2_{i-\frac{1}{2},j+\frac{1}{2}} + \tilde{\Phi}^1_{i-\frac{1}{2},j-\frac{1}{2}}\right) = 0. \tag{3.8}$$

We again use a third order TVD Runge–Kutta scheme for the pseudo time discretization. As in the one-dimensional case, a steady state of Eq. (3.8) may not imply a zero cell residual $\Phi_{i+\frac{1}{2},j+\frac{1}{2}} = 0$ for all i,j, and $\Phi_{i+\frac{1}{2},j+\frac{1}{2}}$ may not be small around sharp gradients even if the steady state solution of Eq. (3.8) is reached. Moreover, we may lose the strict residual property after adding dissipation residuals, but note that conservation is still preserved after adding the dissipation since $\sum_{k=1}^4 \Phi^k_{\text{diss}} = 0$. In addition, the residual property is maintained in smooth regions. It might be possible to improve upon the design of these dissipation residuals to remove their negative effect on local residual property, along the lines of [1] and [6]. This will be investigated in the future. Convergence towards weak solutions in this case relies on a Lax-Wendroff type theorem, and the proof is provided in Appendix. We remark here that in the proof, due to some technical difficulties, we additionally assume uniform or smoothly varying meshes and linear integration in residual evaluation of the diffusion terms. Those assumptions do not seem necessary according to our numerical experiments, and we are still exploring a proof for a more general setting. The numerical results presented in this paper are mostly performed on non-smooth meshes, all with WENO weights in the integration associated with the diffusion terms.

We now summarize the procedure of the high order RD finite difference WENO scheme for two-dimensional scalar steady state problems:

1. Compute the residuals (3.2) using WENO integration and linear interpolation for the derivatives with a proper accuracy.
2. Distribute the residuals according to Eq. (3.3).
3. Revise the residuals by adding a dissipation residual (3.6).
4. Update the point values through sending the residuals and forward in pseudo time (3.8) by a TVD Runge–Kutta time discretization until the steady state is reached.

3.2. Two-dimensional systems

Consider a two-dimensional steady state system (3.1) where u, $f(u)$, $g(u)$ and $h(u,x,y)$ are vector-valued functions in $\mathbb{R}^m$. The viscosity coefficient v is a semi-positive definite matrix. For convection–diffusion systems, we assume that any real linear combination of the Jacobians $\xi_1 f'(u) + \xi_2 g'(u)$ is diagonalizable with real eigenvalues. In particular, we assume $f'(u)$ and $g'(u)$ can be written as $L_x \Lambda_x R_x$ and $L_y \Lambda_y R_y$, respectively, where Λ_x and Λ_y are diagonal matrices with real eigenvalues on the diagonal, and L_x, R_x and L_y, R_y are matrices of left and right eigenvectors for the corresponding Jacobians.

The grid, the grid function and the control volumes are denoted as in Section 3.1. The residual in the cell $I_{i+\frac{1}{2},j+\frac{1}{2}} = [x_i, x_{i+1}] \times [y_j, y_{j+1}]$ is still defined by (3.2). As before, if we reach the zero cell residual limit of the scheme, the accuracy of the scheme is determined by the accuracy of the approximations to the integrations and the derivatives. We again use a fourth order central WENO integration, and fourth order central linear interpolation to approximate the derivatives. For simplicity and without ambiguity, we drop the subscript $(i+\frac{1}{2}, j+\frac{1}{2})$ in the residuals in the following.

We would distribute the residual Φ to the four vertices $\{M_l\}_{l=1,\ldots,4}$, defined in Section 3.1, and the corresponding residuals are still denoted by $\{\Phi^l\}_{l=1,\ldots,4}$, where $\Phi^l \in \mathbb{R}^m$. We also require $\Phi = \sum_{l=1}^4 \Phi^l$ and the residual property that $|\Phi^l|/|\Phi|$ should stay uniformly bounded. Here we consider a dimension by dimension

procedure, coupled with a local characteristic field decomposition. First, we compute an average state $\bar{u}$ in $I_{i+\frac{1}{2},j+\frac{1}{2}}$, using either the simple arithmetic mean or a Roe's average [19], and denote $\bar{L}_x$ and $\bar{R}_x$ as the matrices with left and right eigenvectors L_x and R_x of $f'(u)$ evaluated at the average state, and $\bar{\lambda}_x^m$ the corresponding eigenvalues; $\bar{L}_y$, $\bar{R}_y$ and $\bar{\lambda}_y^m$ are defined similarly but associated with L_y, R_y and Λ_y of $g'(u)$.

We first consider the x-direction and project the residual Φ to the x-characteristic fields: $\Psi = \bar{R}_x\Phi$. The residual Ψ is to be split into two parts in the x-direction: one is Ψ^+, which is sent to the side x_{i+1}; the other is Ψ^-, sent to the side x_i, and $\Psi = \Psi^+ + \Psi^-$. $\Psi^\pm$ are defined by

$$\Psi^+ = \Sigma\Psi, \quad \Psi^- = (I - \Sigma)\Psi, \tag{3.9}$$

where I is the identity matrix and Σ is a diagonal matrix with the mth diagonal component

$$\Sigma_{mm} = \frac{\alpha_m + \frac{k|v|}{2(|\bar{\lambda}_x^m|+\epsilon)\Delta x_{i+\frac{1}{2}}}}{1 + \frac{k|v|}{(|\bar{\lambda}_x^m|+\epsilon)\Delta x_{i+\frac{1}{2}}}} \tag{3.10}$$

with $|v|$ the spectral radius of the matrix v, and ϵ taken as 10^{-6} to avoid the denominator to be zero. The number α_m is the distribution coefficient associated with convection in mth x-characteristic field

$$\alpha_m = \begin{cases} 1, & \text{if } \bar{\lambda}_x^m \geqslant \varepsilon, \\ 0, & \text{if } \bar{\lambda}_x^m \leqslant -\varepsilon, \\ r(\bar{\lambda}_x^m, \varepsilon), & \text{otherwise.} \end{cases}$$

with the function $r(\cdot,\cdot)$ defined by Eq. (2.8) and ε chosen accordingly in the problem. Then we project $\Psi^\pm$ back to the physical space to obtain $\hat{\Phi}^\pm$

$$\hat{\Phi}^+ = \bar{L}_x\Psi^+, \quad \hat{\Phi}^- = \bar{L}_x\Psi^-.$$

Next, we consider the y-direction, and we would distribute the two parts $\hat{\Phi}^\pm$ in the y-direction. We first project $\hat{\Phi}^\pm$ to the y-characteristic fields to obtain $\Pi^\pm$

$$\Pi^+ = \bar{R}_y\hat{\Phi}^+, \quad \Pi^- = \bar{R}_y\hat{\Phi}^-.$$

Then we distribute $\Pi^\pm$ in the y-characteristic fields as follows:

$$\bar{\Psi}^1 = \Gamma\Pi^+, \quad \bar{\Psi}^2 = (I - \Gamma)\Pi^+, \quad \bar{\Psi}^3 = \Gamma\Pi^-, \quad \bar{\Psi}^4 = (I - \Gamma)\Pi^-, \tag{3.11}$$

where I is the identity matrix and Γ is a diagonal matrix with the mth diagonal component

$$\Gamma_{mm} = \frac{\beta_m + \frac{k|v|}{2(|\bar{\lambda}_y^m|+\epsilon)\Delta y_{j+\frac{1}{2}}}}{1 + \frac{k|v|}{(|\bar{\lambda}_y^m|+\epsilon)\Delta y_{j+\frac{1}{2}}}} \tag{3.12}$$

with $|v|$ and ϵ defined as in Eq. (3.10). The number β_m is the distribution coefficient associated with convection in mth y-characteristic field

$$\beta_m = \begin{cases} 1, & \text{if } \bar{\lambda}_y^m \geqslant \varepsilon, \\ 0, & \text{if } \bar{\lambda}_y^m \leqslant -\varepsilon, \\ r(\bar{\lambda}_y^m, \varepsilon), & \text{otherwise.} \end{cases}$$

Finally, we project the distributed residuals back to the physical space

$$\Phi^l = \bar{L}_y\bar{\Psi}^l, \quad l = 1, \ldots, 4.$$

As in the scalar case, we add a dissipation residual Φ^l_{diss} to each of Φ^l around the sharp gradients. The dissipation residuals are defined in Eq. (3.6). We define the distributed residuals by $\tilde{\Phi}^l = \Phi^l + \theta\Phi^l_{\text{diss}}$, $l = 1, \ldots, 4$, where θ is the discontinuity indicator given in Eq. (3.7).

The point value u_{ij} is then updated through sending the distributed residuals to the point (x_i, y_j), as in a pseudo time-marching scheme, which can be written as the semi-discrete system (3.8). We again use a third order TVD Runge–Kutta scheme for the pseudo time discretization.

We now summarize the procedure of the high order RD finite difference WENO scheme for two-dimensional steady state systems:

1. Compute the residuals defined in Eq. (3.2) using WENO integration and linear interpolation for the derivatives with a proper accuracy.
2. Project the residuals to the local x-characteristic fields.
3. Distribute the residuals in the x-direction according to Eq. (3.9), and transform the two parts of residuals back to the physical space.
4. Project the residuals to the local y-characteristic fields.
5. Distribute the residuals in the y-direction, according to Eq. (3.11), and transform the four distributed residuals back to the physical space.
6. Revise the residuals by adding a dissipation residual.
7. Update the point values through sending the residuals and forward in pseudo time (3.8) by a TVD Runge–Kutta time discretization until the steady state is reached.

As before, conservation is still preserved after adding the dissipation since $\sum_{l=1}^{4} \Phi^l_{\text{diss}} = 0$. In addition, the residual property is maintained in smooth regions.

4. Numerical results

In this section we provide numerical experimental results to demonstrate the good behavior of our schemes. Pseudo time discretization towards steady state is by the third order TVD Runge–Kutta method in all numerical simulations. The time step Δt is defined by $\frac{\text{CFL}\ \Delta^2}{\lambda\Delta+\mu}$, where $\Delta = \min\{\Delta x, \Delta y\}$, λ is the maximum of the local speed, μ is the maximum diffusion coefficient, and the CFL number is taken to be 0.2 in our test cases. In Sections 4.1 and 4.2, for one-dimensional problems, the parameter ε in Eq. (2.8) for Roe's entropy correction is taken as 0. In Sections 4.3 and 4.4, for two-dimensional problems, ε is taken as 0.01 unless otherwise stated. The constants k in the distribution coefficients, Eqs. (2.7), (2.16), (3.4), (3.5), (3.10) and (3.12), are taken to be 0.5 for all cases. This choice is somewhat arbitrary, other choices of k, such as $k = 1$, also work well in our numerical test. We have not pursued the issue of an optimal or universal k in this paper.

4.1. One-dimensional scalar problems

In this subsection, numerical steady state is obtained with L^1 nodal residue reduced to the round-off level.

Example 4.1.1. We solve the steady state solution of the one-dimensional advection–diffusion equation

$$u_t + u_x = \nu u_{xx}$$

with the initial condition

$$u(x,0) = e^{\frac{x-1}{\nu}}, \quad x \in [0,1]$$

which is itself a steady state solution. The boundary conditions are $u(0,t) = 0$ and $u(1,t) = 1$. The viscosity coefficient ν is taken as 0.05. This problem has a boundary layer around $x = 1$. We test our scheme on both uniform meshes and non-uniform meshes. The non-uniform mesh has two distinct mesh sizes, Δx_1 in the interval [0.8,1], and $\Delta x_2 = 4\Delta x_1$ in [0,0.8]. The numerical results are shown in Table 1. We can see clearly that fourth order accuracy is achieved and the magnitudes of the errors on non-uniform meshes are significantly smaller than those on uniform meshes. This demonstrates the capability of the scheme to resolve the boundary layer by locally refining the mesh.

Table 1
Errors and numerical orders of accuracy of the fourth order RD finite difference WENO scheme for Example 4.1.1 on non-uniform and uniform meshes with N cells

N	Non-uniform mesh				Uniform mesh			
	L^1 error	Order	L^∞ error	Order	L^1 error	Order	L^∞ error	Order
20	1.51E − 04	–	3.84E − 04	–	1.70E − 03	–	1.37E − 02	–
40	1.10E − 05	3.78	4.84E − 05	2.99	1.10E − 04	3.95	7.96E − 04	4.11
80	7.63E − 07	3.85	4.22E − 06	3.52	6.83E − 06	4.01	5.04E − 05	3.98
160	5.08E − 08	3.91	3.12E − 07	3.76	4.20E − 07	4.02	3.10E − 06	4.02
320	3.29E − 09	3.95	2.11E − 08	3.89	2.59E − 08	4.02	1.91E − 07	4.02

Example 4.1.2. We consider the steady state solution of the viscous Burgers equation with a source term

$$u_t + \left(\frac{u^2}{2}\right)_x = \nu u_{xx} - \pi \cos(\pi x) u, \quad x \in [0,1]$$

equipped with the boundary condition $u(0,t) = 1$ and $u(1,t) = -0.1$. The viscosity coefficient ν is taken as 0.01. The initial condition is given by

$$u(x,0) = \begin{cases} 1, & \text{if } 0 \leqslant x < 0.3, \\ -0.1, & \text{if } 0.3 \leqslant x < 1. \end{cases}$$

We test our scheme on a non-uniform mesh with two distinct mesh sizes, Δx_1 in the interval [0.1,0.3] and $\Delta x_2 = 4\Delta x_1$ in the remaining part of the domain. The numerical result and the reference solution computed from fifth order finite difference WENO scheme [12] with a fourth order central discretization for the viscous term are displayed in Fig. 1. We can see the good resolution of the inner layer.

4.2. One-dimensional systems

In this subsection, the numerical steady state is obtained with L^1 nodal residue reduced to the round-off level.

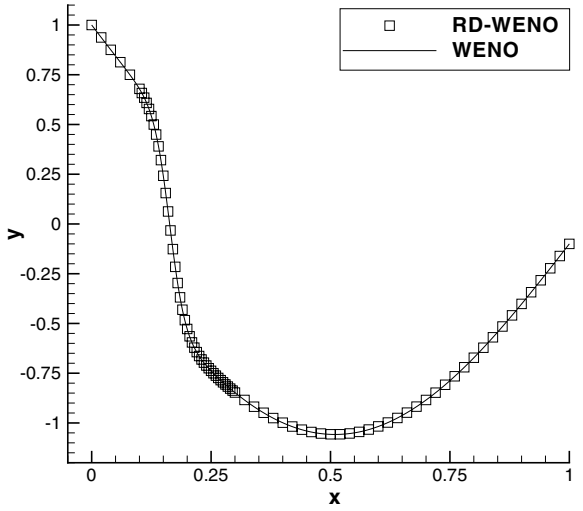

Fig. 1. Reference solution computed from finite difference WENO scheme with 500 points (solid line), and numerical solution computed from RD finite difference (symbols) on non-uniform mesh with 80 cells for Example 4.1.2.

Example 4.2.1. We solve the steady state solution of the one-dimensional Navier–Stokes equations with a source term on $[0, 2\pi]$

$$\begin{pmatrix} \rho \\ \rho u \\ E \end{pmatrix}_t + \begin{pmatrix} \rho u \\ \rho u^2 + p \\ u(E+p) \end{pmatrix}_x = \begin{pmatrix} 0 \\ \frac{1}{Re}\frac{4}{3}u_{xx} + (\gamma-1)\cos x(4+2\sin x) \\ \frac{1}{Re}\frac{2}{3}(u^2)_{xx} + \frac{1}{Re}\frac{1}{(\gamma-1)Pr}\left(\frac{\gamma p}{\rho}\right)_{xx} + \frac{\gamma}{RePr}\sin x \end{pmatrix},$$

where ρ denotes the density, u is the velocity of the fluid, E is the total energy and $p = (\gamma-1)(E - \frac{1}{2}\rho u^2)$ is the pressure. The gas constant γ is taken as 1.4, the Reynolds number Re is 200, and Pr is the Prandtl number taken as 0.72.

Starting from a stationary initial condition $(\rho, \rho u, E) = (2 + \sin x, 0, (2 + \sin x)(1 + 2 + \sin x))$ equipped with a periodic boundary condition, we can check the order of accuracy.

We test our scheme on uniform meshes as well as on non-smooth meshes which are 20% randomly perturbed form the uniform ones. The integration of the source term is evaluated exactly. The numerical results are shown in Table 2. We can clearly see the fourth order accuracy, and the errors on these two types of meshes are comparable.

Example 4.2.2. We test our scheme on the steady state solution of the one-dimensional nozzle flow problem on $[0, 1]$

$$\begin{pmatrix} \rho \\ \rho u \\ E \end{pmatrix}_t + \begin{pmatrix} \rho u \\ \rho u^2 + p \\ u(E+p) \end{pmatrix}_x = -\frac{a'(x)}{a(x)}\begin{pmatrix} \rho u \\ \rho^2 u^2/\rho \\ u(E+p) \end{pmatrix} + \frac{1}{Re}\begin{pmatrix} 0 \\ \frac{4}{3}u_{xx} \\ \frac{2}{3}(u^2)_{xx} + \frac{1}{(\gamma-1)Pr}\left(\frac{\gamma p}{\rho}\right)_{xx} \end{pmatrix},$$

where $a(x)$ represents the area of the cross section of the nozzle and other variables are defined as in Example 4.2.1. The Reynolds number Re is 400, and Pr is Prandtl number taken as 0.72.

We start with an isentropic initial condition, with a shock at $x = 0.5$. The density ρ and pressure p at $-\infty$ are 1, and the inlet Mach number at $x = 0$ is 0.8. The outlet Mach number at $x = 1$ is 1.8, with linear Mach number distribution before and after the shock. The area of the cross section $a(x)$ is then determined by the relation

$$a(x) f(\text{Mach number at } x) = \text{constant}, \quad \forall x \in [0, 1],$$

where

$$f(w) = \frac{w}{(1 + \delta w^2)^p}, \quad \delta = \frac{1}{2}(\gamma - 1), \quad p = \frac{1}{2}\cdot\frac{\gamma+1}{\gamma-1}.$$

We test our scheme on a non-uniform mesh with two distinct mesh sizes, Δx_1 in the interval [0.4,0.6], and $\Delta x_2 = 4\Delta x_1$ in the remaining part of the domain.

Table 2
Errors and numerical orders of accuracy for the density ρ of the fourth order RD finite difference WENO scheme for Example 4.2.1 on non-smooth and uniform meshes with N cells

N	Non-smooth mesh				Uniform mesh			
	L^1 error	Order	L^∞ error	Order	L^1 error	Order	L^∞ error	Order
20	2.32E − 04	–	3.48E − 04	–	2.03E − 04	–	3.21E − 04	–
40	1.31E − 05	4.14	2.03E − 05	4.10	1.29E − 05	3.98	2.02E − 05	3.99
80	8.17E − 07	4.01	1.28E − 06	3.99	8.06E − 07	4.00	1.27E − 06	4.00
160	5.06E − 08	4.01	7.95E − 08	4.01	4.87E − 08	4.05	7.70E − 08	4.04
320	1.45E − 09	5.12	3.12E − 09	4.67	1.52E − 09	5.00	3.78E − 09	4.35

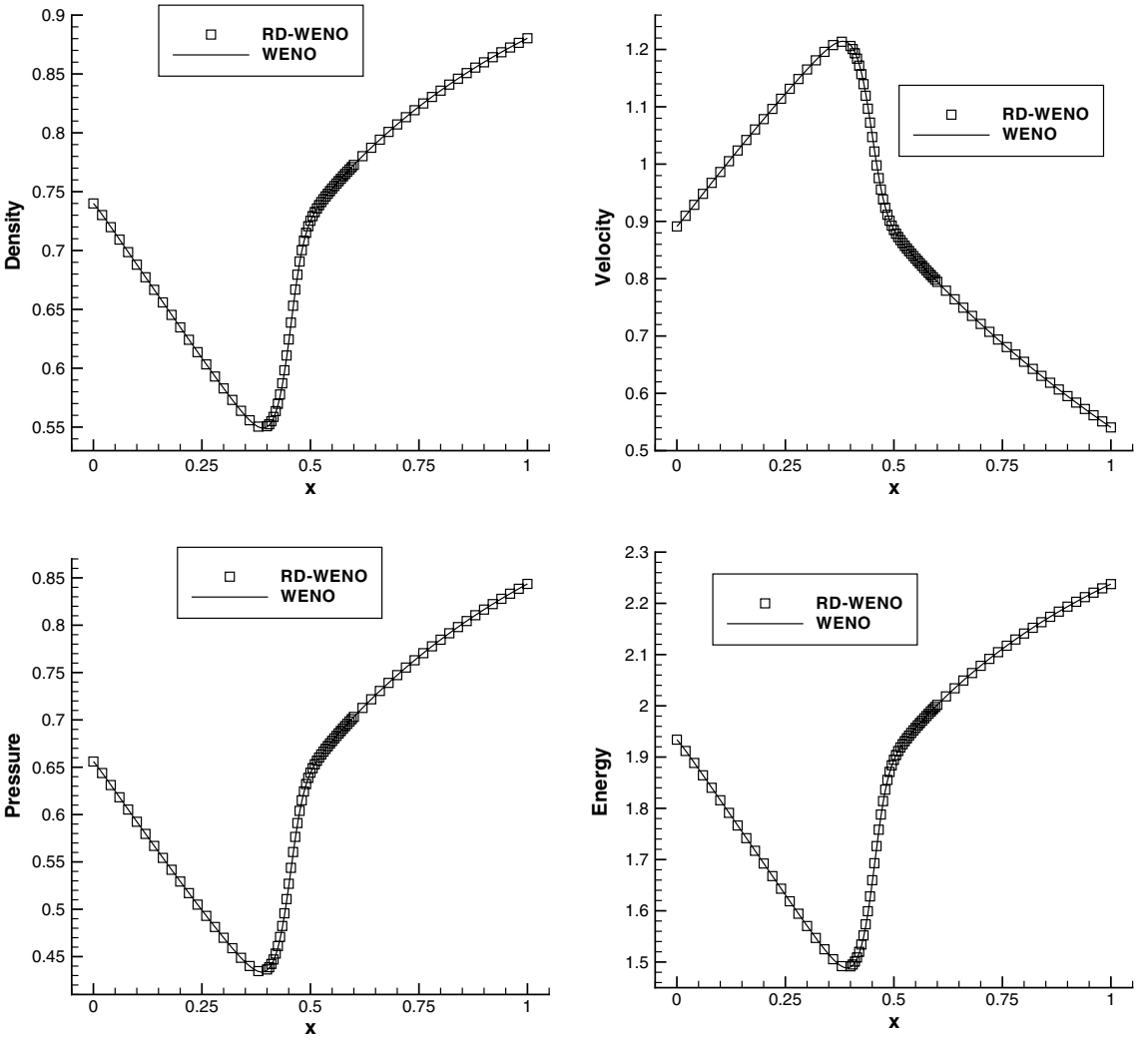

Fig. 2. Nozzle flow problem. Solid lines: finite difference WENO scheme on a uniform mesh with 200 points; symbols: RD finite difference scheme on a non-uniform mesh with 80 points. Top left: density; top right: velocity; bottom left: pressure; bottom right: total energy.

We compare our numerical solution with the reference solution computed from fifth order finite difference WENO scheme with fourth order central discretization for the viscous terms using 200 points. From Fig. 2, we can see that the inner layer is resolved well.

Example 4.2.3. We solve the steady state solution of the one-dimensional semiconductor hydrodynamic (HD) model, see [11]

$$\begin{pmatrix} n \\ p \\ W \end{pmatrix}_t + \begin{pmatrix} nv \\ pv + knT \\ v(W + knT) \end{pmatrix}_x = \begin{pmatrix} 0 \\ en\phi_x - \frac{p}{\tau_p} \\ env\phi_x - \frac{W - W_0}{\tau_w} \end{pmatrix} + \begin{pmatrix} 0 \\ 0 \\ \kappa T_x \end{pmatrix}_x.$$

The electric field $-\phi_x$ is obtained from the Poisson equation

$$\phi_{xx} = \frac{e}{\epsilon}(n - n_d).$$

Here, n denotes the electron concentration, v is the velocity, W is the total energy, and $e = 0.1602$ is the charge of the electron. The momentum p is related to v by $p = mnv$, where m is the electron mass taken as 0.26×0.9190, and the temperature T is related to the total energy by

$$W = \frac{3}{2}knT + \frac{1}{2}mnv^2$$

and $k = 0.138 \times 10^{-4}$ is the Boltzmann constant. The momentum and energy relaxation times are given by $\tau_p = C_p \frac{T_0}{T}$ and $\tau_w = C_w \frac{T}{T+T_0} + \frac{1}{2}\tau_p$, where C_p and C_w are constants determined by

$$C_p = \frac{m}{e}\mu_0, \quad C_w = \frac{3\mu_0 k T_0}{2ev_s^2}$$

with $\mu_0 = 0.14$ for the HD model and $v_s = 0.1$ in our unit. The thermal conductivity κ is governed by the Wiedemann-Franz law, described by $\kappa = \frac{3}{2}n\frac{k^2\mu_0 T_0}{e}$.

The silicon diode we simulate has a length of 0.6 μm with a doping defined by $n_d = 5 \times 10^{17}\ \mathrm{cm}^{-3}$ in $[0, 0.1]$ and in $[0.5, 0.6]$ and $n_d = 3 \times 10^{15}\ \mathrm{cm}^{-3}$ in $[0.15, 0.45]$, with a smooth transition in between. The lattice temperature is taken as $T_0 = 300$ K.

The boundary conditions are given as follows: $\phi = \phi_0 = \frac{kT}{e}\log(\frac{n_d}{n_i})$ at the left boundary, with $n_i = 1.4 \times 10^{10}\ \mathrm{cm}^{-3}$, $\phi = \phi_0 + \mathrm{vbias}$ with the voltage drop $\mathrm{vbias} = 1.5$ at the right boundary for the potential; $T = 300$ K at both boundaries for the temperature; $n = 5 \times 10^{17}\ \mathrm{cm}^{-3}$ at both boundaries for the concentration; and a Neumann boundary condition is used for the velocity v at both boundaries.

We test our scheme on a non-uniform mesh with two distinct mesh sizes, Δx_1 in the interval $[0.05, 0.15]$ and $[0.45, 0.55]$ near the junctions, and $\Delta x_2 = 4\Delta x_1$ in the remaining part of the domain. In Fig. 3, we compare our results with the solution computed from third order ENO finite difference scheme [11]. We can see that the overshoot is captured very well. In this particular case, we need extra dissipation to stabilize the system. The artificial dissipation is added through a one-dimensional discontinuity indicator, as described in Section 3.1, and the coefficient δ for the dissipation (3.6) is taken as 10.

4.3. Two-dimensional scalar problems

In this subsection, numerical steady state is obtained with L^1 nodal residue reduced to the round-off level.

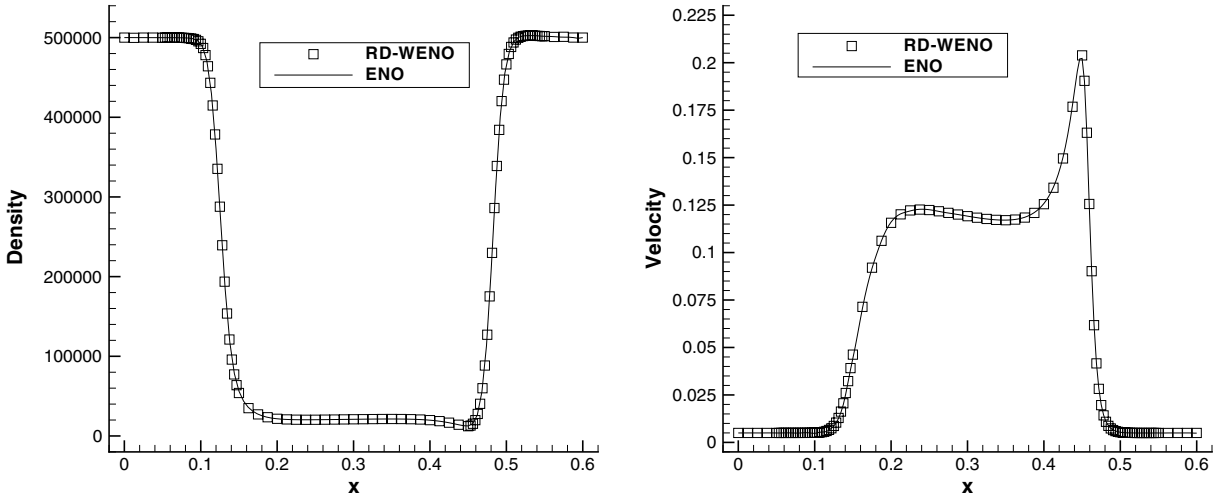

Fig. 3. Semiconductor HD model. Solid lines: finite difference ENO scheme on uniform mesh with 192 points; symbols: RD finite difference scheme on non-uniform mesh with 96 points. Left: density; right: velocity.

Example 4.3.1. We solve the steady state problem of two-dimensional advection–diffusion equation

$$u_t + u_x + u_y = v(u_{xx} + u_{yy}), \quad (x, y) \in [0, 1] \times [0, 1]$$

with the initial condition given by

$$u(x, y, 0) = e^{\frac{x-1}{v} + \frac{y-1}{v}}$$

which is itself a steady state solution. The viscosity coefficient v is taken as 0.05, and the exact solution is imposed on the boundaries.

This problem has boundary layers along $x = 1$ and $y = 1$. For this example, the parameter ε in (2.8) for Roe's entropy correction is taken as 0. We test our scheme on both uniform meshes and non-uniform meshes. The non-uniform mesh has two distinct mesh sizes, Δx_1, Δy_1 in the interval $[0.8, 1.0]$, and $\Delta x_2 = 4\Delta x_1$, $\Delta y_2 = 4\Delta y_1$ in $[0, 0.8]$.

For an example of the non-uniform mesh, see Fig. 4. The numerical results are shown in Table 3. We can see clearly that fourth order accuracy is achieved, with magnitudes of the errors on non-uniform meshes significantly smaller than those on uniform meshes. This demonstrates the capability of the scheme to resolve the boundary layers.

Example 4.3.2. We consider the one-dimensional viscous Burgers equation viewed as a two-dimensional steady state problem

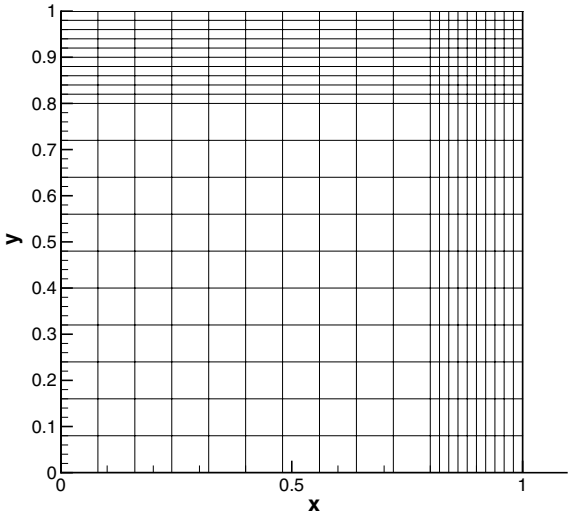

Fig. 4. A demonstration of the non-uniform mesh with 20×20 cells.

Table 3
Errors and numerical orders of accuracy of the fourth order RD finite difference WENO scheme for Example 4.3.1 on non-uniform and uniform meshes with $N \times N$ cells

$N \times N$	Non-uniform mesh				Uniform mesh			
	L^1 error	Order	L^∞ error	Order	L^1 error	Order	L^∞ error	Order
20×20	8.89E − 06	–	1.37E − 04	–	4.26E − 05	–	4.49E − 03	–
40×40	7.89E − 07	3.49	7.14E − 06	4.26	3.32E − 06	3.68	3.68E − 04	3.61
80×80	6.70E − 08	3.56	7.27E − 07	3.30	2.14E − 07	3.96	1.96E − 05	4.23
160×160	4.93E − 09	3.76	6.15E − 08	3.56	1.31E − 08	4.03	1.17E − 06	4.06
320×320	3.38E − 10	3.87	4.57E − 09	3.75	7.98E − 10	4.04	6.95E − 08	4.07

$$u_t + \left(\frac{u^2}{2}\right)_x + u_y = \nu u_{xx}, \quad (x,y) \in [-0.2, 0.2] \times [0, 0.4]. \tag{4.1}$$

This problem has the steady state solution

$$u(x,y,\infty) = \frac{-4\sinh(\frac{y+2x}{\nu})}{\cosh(\frac{y+2x}{\nu}) + e^{\frac{1}{(200\nu-4y)\nu}}} - \frac{1}{2}$$

with the exact solution imposed on the boundaries.

The viscosity coefficient ν is taken as 0.05. We start from an initial condition $u(x,y,0) = u(x,0,0)$ and march to steady state by a pseudo-time marching. We test our scheme on both uniform and non-smooth meshes. The non-smooth meshes are 20% randomly perturbed from the uniform ones. Table 4 shows fourth order accuracy for both meshes, and the magnitude of the errors are comparable. The three-dimensional plot of the numerical solution on a non-smooth mesh with 80×80 cells and the cross sections at $y = 0.1, 0.2, 0.3$ compared with the exact solution are displayed in Fig. 5. We can clearly observe good resolution of the numerical scheme for this example. The coefficient δ for the dissipation (3.6) is taken as 0.

Example 4.3.3. We again consider Eq. (4.1) on the domain $[0,1]\times[0,1]$ with the boundary conditions

$$u(x,0,t) = 1.5 - 2x, \quad u(0,y,t) = 1.5, \quad u(1,y,t) = -0.5.$$

The viscosity coefficient ν is taken as 0.02. We start from an initial condition $u(x,y,0) = u(x,0,0)$ and march to steady state by a pseudo-time marching. We solve the one-dimensional Burgers equation by using fifth order finite difference WENO scheme with a fourth order central discretization for the viscous term with 500 points and compare with our numerical solution. In Fig. 6, the three-dimensional plot of the numerical solution and the cross sections at $y = 0.25, 0.5, 0.75$ are displayed. We can clearly observe good resolution of the numerical scheme compared with the reference solution. The coefficient δ for the dissipation (3.6) is taken as 10.

Example 4.3.4. We consider the steady state solution of the following problem on $[0, 1/\sqrt{2}] \times [0, 1/\sqrt{2}]$

$$u_t + \left(\frac{1}{\sqrt{2}}\frac{u^2}{2}\right)_x + \left(\frac{1}{\sqrt{2}}\frac{u^2}{2}\right)_y = (2\sqrt{2}(x+y) - 2)u + \nu(u_{xx} + u_{yy}).$$

The boundary conditions are given as follows for point (x,y) on the boundary, with $w = (x+y)/\sqrt{2}$,

$$u(x,y,t) = \begin{cases} 1 - 2w + 2w^2, & \text{if } 0 \leqslant w \leqslant 0.3419, \\ -0.1 - 2w + 2w^2, & \text{otherwise.} \end{cases}$$

The initial condition is

Table 4
Errors and numerical orders of accuracy of the fourth order RD finite difference WENO scheme for Example 4.3.2 on non-uniform and uniform meshes with $N \times N$ cells

$N \times N$	Non-uniform mesh				Uniform mesh			
	L^1 error	Order	L^∞ error	Order	L^1 error	Order	L^∞ error	Order
20×20	1.16E − 02	–	1.44E − 01	–	1.09E − 02	–	1.44E − 01	–
40×40	1.16E − 03	3.32	1.85E − 02	2.96	1.10E − 03	3.31	1.72E − 02	3.06
80×80	7.30E − 05	3.99	1.12E − 03	4.04	7.08E − 05	3.96	1.26E − 03	3.77
160×160	4.57E − 06	4.00	8.13E − 05	3.79	4.50E − 06	3.98	8.46E − 05	3.90

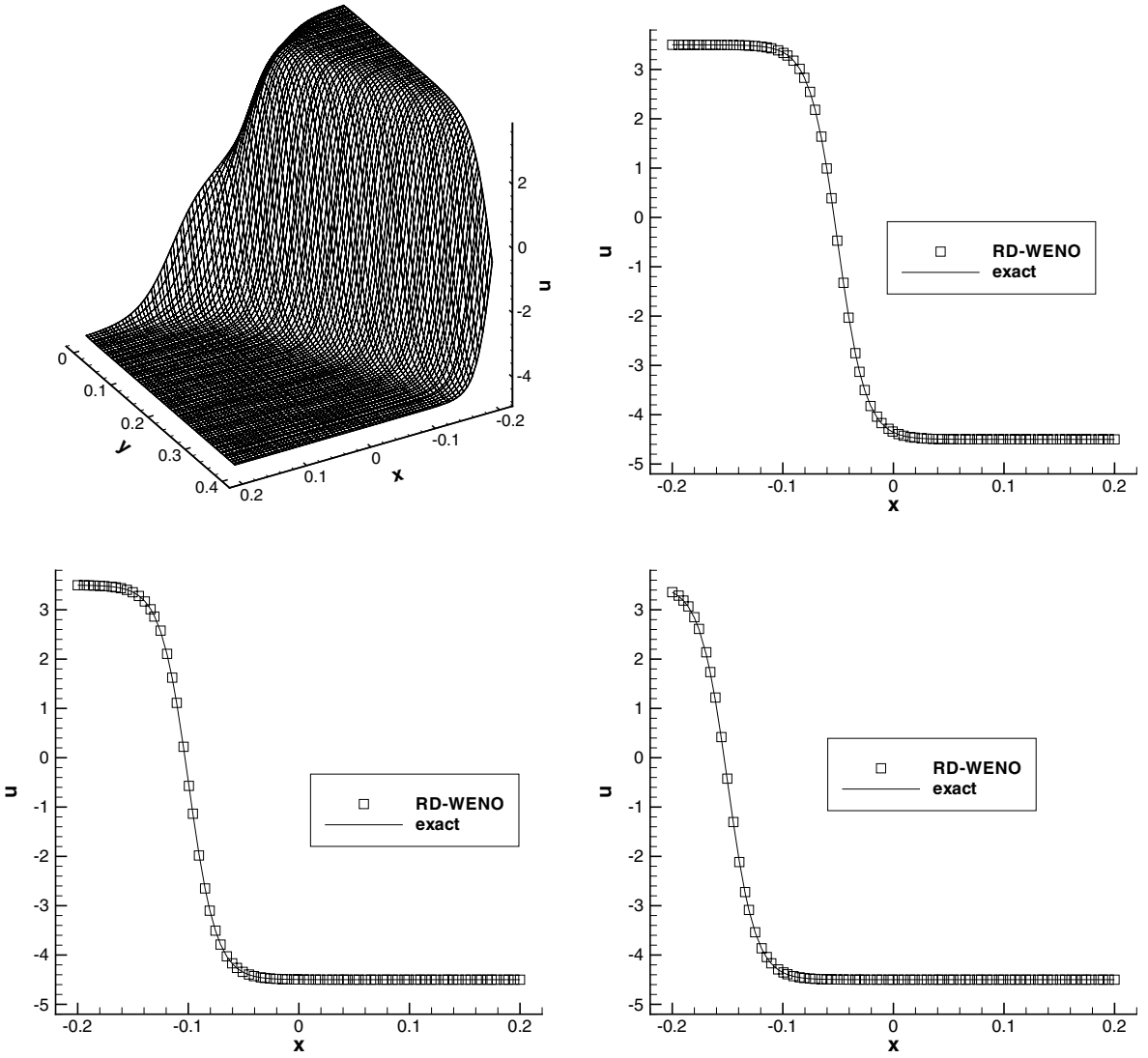

Fig. 5. Example 4.3.2. Non-smooth mesh with 80×80 cells. Top left: three-dimensional plot; top right: cross section at $y = 0.1$; bottom left: cross section at $y = 0.2$; bottom right: cross section at $y = 0.3$. For the cross sections, the solid lines are for the exact solution and symbols are for the numerical solution.

$$u(x,y,0) = \begin{cases} 1, & \text{if } 0 \leqslant w < 0.3, \\ -0.1, & \text{if } 0.3 \leqslant w < 1, \end{cases}$$

and the viscous coefficient is taken as 0.01. We test our scheme on a non-smooth mesh which is 20% randomly perturbed from the uniform one.

The coefficient δ for the dissipation (3.6) is taken as 10. The 3D plot for (x,y) in $[0.06, 0.7] \times [0.06, 0.7]$ and the cross section along the diagonal is displayed in Fig. 7.

4.4. Two-dimensional systems

In our numerical tests in this subsection, the L^1 nodal residue can only be reduced to around 10^{-3}–10^{-5} and then stagnates at that level. This might be related to the boundary conditions or lack of suitable numerical dissipation in certain regimes. More study is needed to address this issue.

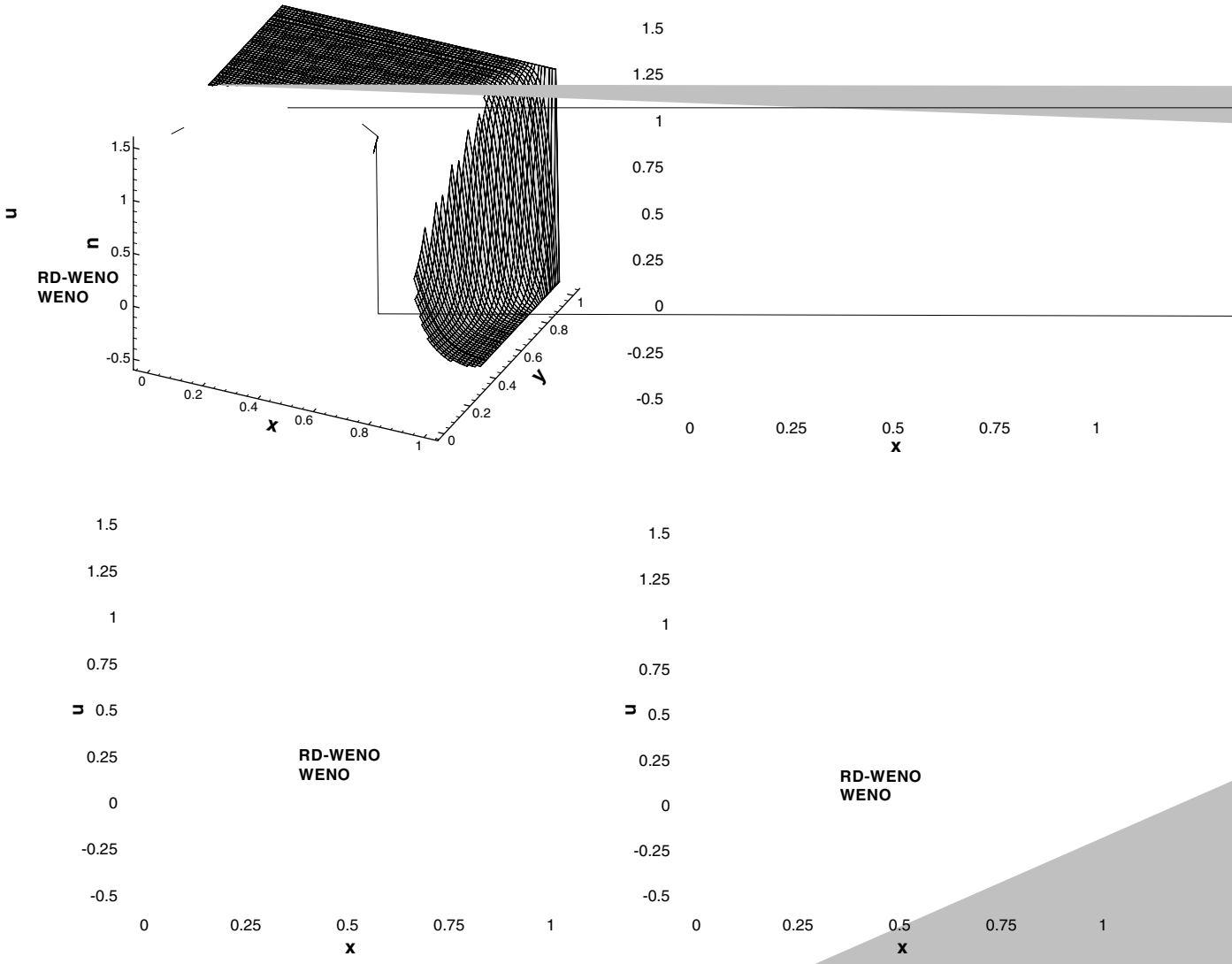

Fig. 6. Example 4.3.3. Numerical solutions from finite difference WENO scheme with 500 points (solid line) and one computed form RD finite difference scheme (symbols) on a non-smooth mesh with 80×80 cells. Top left: three-dimensional plot; top right: cross section at $y = 0.25$; bottom left: cross section at $y = 0.5$; bottom right: cross section at $y = 0.75$.

Example 4.4.1. We consider the two-dimensional Navier–Stokes equations

$$\mathbf{u}_t + \mathbf{f}(\mathbf{u})_x + \mathbf{g}(\mathbf{u})_y = \boldsymbol{v}_1(\mathbf{u})_x + \boldsymbol{v}_2(\mathbf{u})_y, \tag{4.2}$$

where $\mathbf{u} = (\rho,\rho u,\rho v,E)^T$, $\mathbf{f}(u) = (\rho u,\rho u^2 + p,\rho uv,u(E+p))^T$, $\mathbf{g}(u) = (\rho v,\rho uv,\rho v^2 + p,v(E+p))^T$, $\boldsymbol{v}_1(\mathbf{u}) = (0,\tau_{xx},\tau_{xy},u\tau_{xx} + v\tau_{xy} - \chi_x)$, and $\boldsymbol{v}_2(\mathbf{u}) = (0,\tau_{yx},\tau_{yy},u\tau_{yx} + v\tau_{yy} - \chi_y)$.

Here ρ is the density, (u,v) is the velocity, E is the total energy and $p = (\gamma - 1)(E - \frac{1}{2}(\rho u^2 + \rho v^2))$ is the pressure. The gas constant γ is taken as 1.4 in our numerical tests. The variables $\tau_{xx},\tau_{xy},\tau_{yx},\tau_{yy}$ are viscous stresses defined by

$$\tau_{xx} = -\frac{2\mu}{3}(u_x + v_y) + 2\mu u_x, \quad \tau_{xy} = \mu(u_y + v_x) = \tau_{yx}, \quad \tau_{yy} = -\frac{2\mu}{3}(u_x + v_y) + 2\mu u_y$$

and heat flux components χ_x and χ_y are defined by

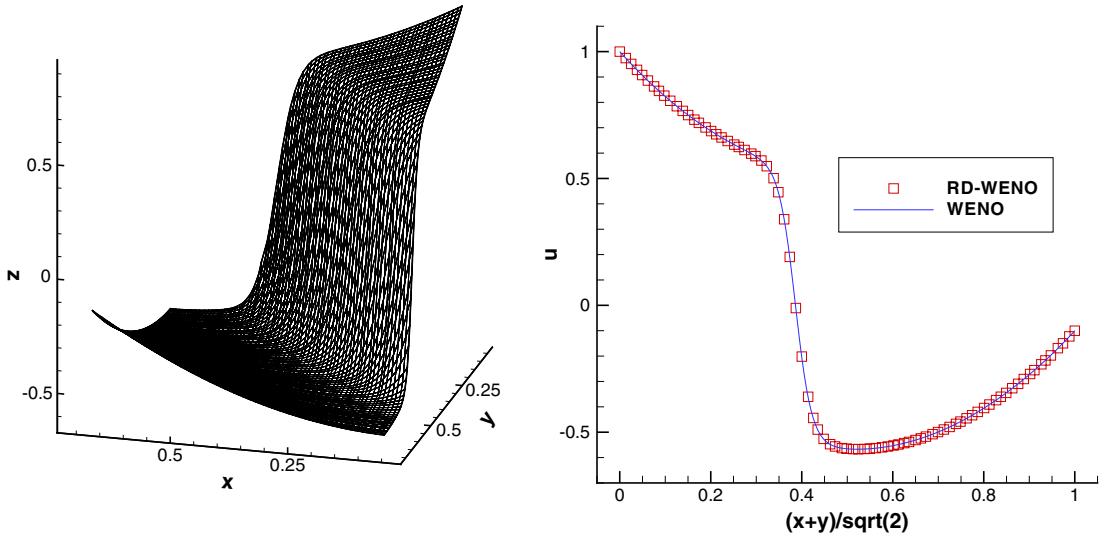

Fig. 7. Example 4.3.4. Non-smooth mesh with 80×80 cells. Left: three-dimensional plot; right: the numerical solution (symbols) versus the reference solution computed by a fifth order finite difference WENO scheme with 200×200 points (solid line) along the cross section through the northeast to southwest diagonal.

$$\chi_x = -\frac{\gamma\mu}{Pr}\left(\frac{p}{(\gamma-1)\rho}\right)_x, \quad \chi_y = -\frac{\gamma\mu}{Pr}\left(\frac{p}{(\gamma-1)\rho}\right)_y,$$

where μ, the viscosity coefficient, is taken as 5×10^{-3} and Pr is the Prandtl number taken as 0.72.

In this example, we consider a flow generated by pressure gradients on the domain $[0,2] \times [-1,1]$. We start with an initial condition where $(\rho,u,v,p) = (1,0.1,0,2.02)$ on $x = 0$ and $(\rho,u,v,p) = (1,0.1,0,2)$ on $x = 1$, with a linear distribution in between. Non-slip boundary conditions are imposed on the $y = -1$ and $y = 1$. The boundary conditions for $x = 0$ and $x = 1$ are given by $(\rho,u,v,p) = (1,0.1,0,2.02)$ and $(1,0.1,0,2)$, respectively. The coefficient δ for the dissipation (3.6) is taken as 5. We test our scheme on a non-smooth mesh which is 20% perturbed form the uniform ones.

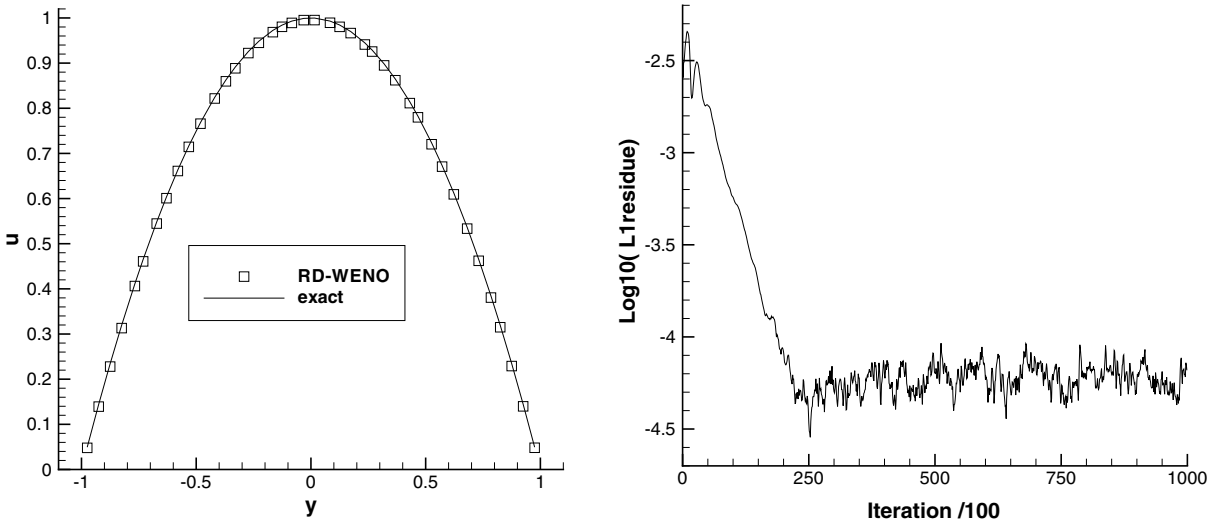

Fig. 8. Example 4.4.1. 40×40 non-smooth mesh. Left: profile of u at $x = 1$ of the numerical solution (symbols) versus that of the analytical solution (solid line); right: The convergence history with L^1 nodal residue.

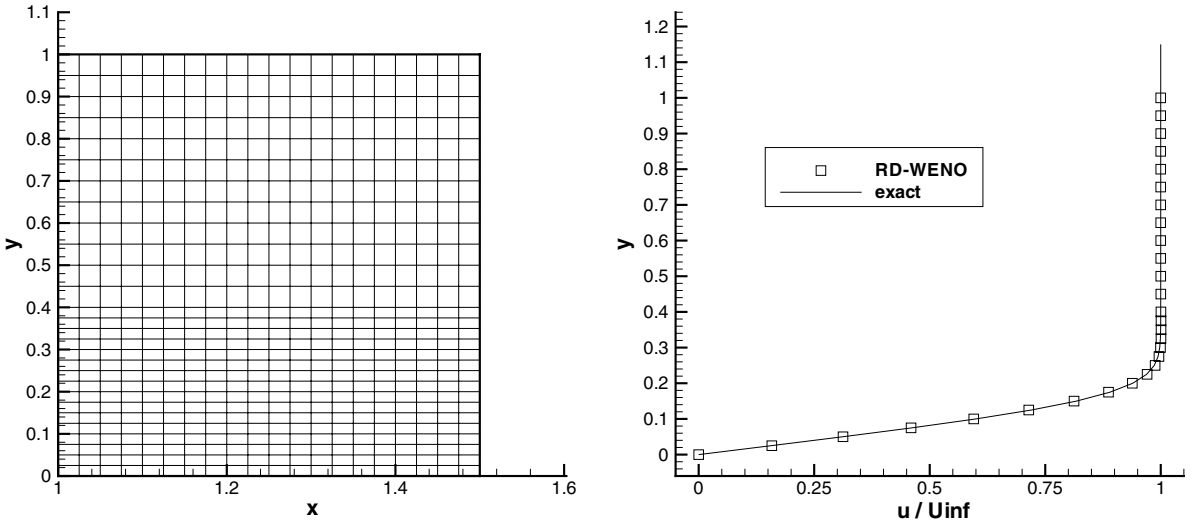

Fig. 9. Flat plate problem. 20×28 non-uniform mesh. Left: a demonstration of the mesh; right: cross sections at $x = 1.4$ of the numerical solution (symbols) versus the analytical solution (solid line).

Since the variation of density is relatively very small, we compare our numerical solution with the analytical solution for incompressible flow. The theoretical profile of u is $\frac{P}{2\mu}(1-y^2)$ for all x in [0,1], where P is the pressure gradient $-\frac{dp}{dx}$. In Fig. 8, we plot the cross sections of both solutions at $x = 1$ and the convergence history with L^1 nodal residue which can only be reduced to the level around 10^{-4} and then stagnates at that level.

Example 4.4.2. We solve the problem of flow passing a flat plate. Steady state solution of the Navier–Stokes Eq. (4.2) is computed on the domain $[1, 1.5] \times [0, 2]$, with the plate on $y = 0$ and viscosity coefficient $\mu = 10^{-3}$. The variables of free stream flow is $(\rho_\infty, u_\infty, v_\infty, p_\infty) = (0.1, 0.5, 0, \frac{1}{\gamma})$. The initial condition is taken as the free stream flow. Due to the low Mach number, the variation of density is negligible, and we simply use the analytical solution for incompressible flow as boundary conditions on the two boundaries $x = 1$ and $x = 1.5$. A non-slip boundary condition is imposed on the lower boundary $y = 0$, and we assume vanishing derivatives on the upper boundary $y = 1$. The coefficient δ for the dissipation (3.6) is taken as 5. We test the problem on a mesh with a uniform discretization in a x direction, but in a y direction, in order to resolve the boundary layer, we use two distinct mesh sizes, Δy_1 in $[0, 0.4]$ and $\Delta y_2 = 2\Delta y_1$ in $[0.4, 1]$. In Fig. 9, we compare the cross sections at $x = 1.4$ of our numerical solution with the analytical solution. In this case, the L^1 nodal residue can only be reduced to the level around 10^{-5} and then stagnates at that level.

Example 4.4.3. We consider Eq. (4.2) on the domain $[0, 4] \times [0, 1]$ with viscosity coefficient $\mu = 2 \times 10^{-3}$. We start with an initial condition where $(\rho, u, v, p) = (1.69997, 2.61934, -0.50632, 1.52819)$ on $y = 4$ and $(\rho, u, v, p) = (1, 2.9, 0, \frac{1}{\gamma})$ otherwise. The boundary conditions are given by $(\rho, u, v, p) = (1.69997, 2.61934, -0.50632, 1.52819)$ on $y = 1$, and a non-slip boundary condition on $y = 0$. The left boundary at $x = 0$ is set as an inflow with $(\rho, u, v, p) = (1, 2.9, 0, \frac{1}{\gamma})$, and the right boundary at $x = 4$ is set to be an outflow with no boundary conditions prescribed (one-sided WENO integration is performed near the right boundary). The coefficient δ for the dissipation (3.6) is taken as 25. We test the problem on a mesh with a uniform discretization in a x direction, but in a y direction, we use two distinct mesh sizes, Δy_1 in $[0, 0.2]$ and $[0.8, 1]$, and $\Delta y_2 = 4\Delta y_1$ in $[0.2, 0.8]$. We use a finer mesh around $y = 0$ and $y = 1$ to resolve the boundary layers. The numerical results are shown in Fig. 10. We can clearly see a good resolution of the layers. In this case, the L^1 nodal residue can only be reduced to the level around 10^{-3} and then stagnates at that level.

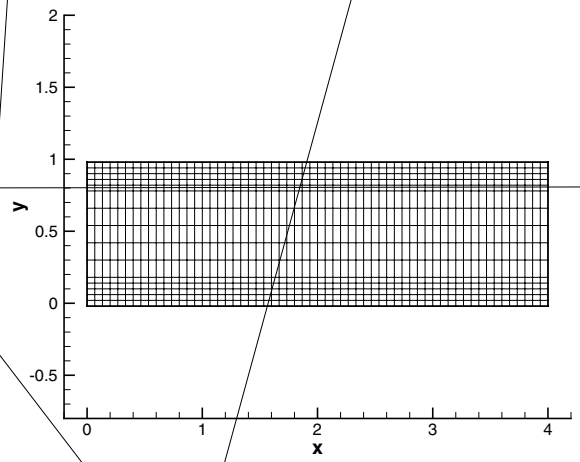

5. Concluding remarks

In this paper we have designed a high order conservative residual distribution finite difference WENO scheme on non-smooth Cartesian meshes for solving steady state solutions of convection–diffusion equations in one and two space dimensions. The restriction on the meshes allows us to compute the residual dimension by dimension to high order accuracy, and hence leads to the savings of computational costs. Without smoothness assumptions on the meshes, we can resolve the inner or boundary layer regions by locally refining the meshes while maintaining high order accuracy. The residual distribution is designed based on weighing the effects of convection and diffusion, and principles are obeyed to ensure high order accuracy at steady state. A Lax-Wendroff type theorem is proved for convergence towards weak solutions in one and two dimensions with additional assumptions. The proof for a more general setting is still under exploration. Numerical experiments are performed to demonstrate the accuracy and good resolution of our scheme around the layers. Generalization of the technique to 3D is straightforward and will be carried out in the future. As mentioned at the beginning of Section 4.4, our scheme still has difficulty in reaching machine zero steady states for two-dimensional systems. Acceleration techniques and improvement on the additional dissipation residual for stabilizing the pseudo time marching, to help the scheme to reach machine zero steady states for multi-dimensional systems, will be explored in the future. Extension of the method for time accurate problems also constitute future work.

Acknowledgments

Research was supported by ARO Grant W911NF-04-1-0291, NSF Grant DMS-0510345 and AFOSR Grant FA9550-05-1-0123.

Appendix A. A Lax-Wendroff type theorem for two dimensions

In this appendix, we state and prove a Lax-Wendroff type theorem for convergence towards weak solutions in the two-dimensional scalar case.

We follow all the notations in Section 3.1. In addition, we define $S^x_{i+\frac{1}{2}} = \{x \mid x \in [x_i, x_{i+1}]\}$, $S^y_{j+\frac{1}{2}} = \{y \mid y \in [y_j, y_{j+1}]\}$, $\Delta x_{i+\frac{1}{2}} = x_{i+1} - x_i$, $\Delta y_{j+\frac{1}{2}} = y_{j+1} - y_j$ and $\Delta x = \max_i \Delta x_i$, $\Delta y = \max_j \Delta y_j$, $\Delta = \max(\Delta x, \Delta y)$. Here we assume $0 < C_1 \leqslant |\Delta x_{i+\frac{1}{2}}/\Delta y_{j+\frac{1}{2}}| \leqslant C_2$ for all i,j. Also we define the function $u_{\Delta x,\Delta y}$ as a piecewise constant function where $u_{\Delta x,\Delta y}(x,y) = u_{ij}$, $(x,y) \in C_{ij}$.

As in Section 3.1, the residual in the cell $I_{i+\frac{1}{2},j+\frac{1}{2}}$ given by (3.2) is approximated by

$$\begin{aligned}\Phi_{i+\frac{1}{2},j+\frac{1}{2}} = {} & \mathscr{R}\left(f(u_{\Delta x,\Delta y}(x_{i+1},y)), S^y_{j+\frac{1}{2}}\right) - \mathscr{R}\left(f(u_{\Delta x,\Delta y}(x_i,y)), S^y_{j+\frac{1}{2}}\right) + \mathscr{R}(g(u_{\Delta x,\Delta y}(x,y_{j+1})), S^x_{i+\frac{1}{2}}) \\ & - \mathscr{R}(g(u_{\Delta x,\Delta y}(x,y_j)), S^x_{i+\frac{1}{2}}) - \mathscr{R}(\mathscr{R}\left(h(u_{\Delta x,\Delta y},x,y), S^y_{j+\frac{1}{2}}\right), S^x_{i+\frac{1}{2}}) - v\bar{\mathscr{R}}\left(\mathscr{D}_x(u_{\Delta x,\Delta y},x_{i+1},y), S^y_{j+\frac{1}{2}}\right) \\ & + v\bar{\mathscr{R}}\left(\mathscr{D}_x(u_{\Delta x,\Delta y},x_i,y), S^y_{j+\frac{1}{2}}\right) - v\bar{\mathscr{R}}(\mathscr{D}_y(u_{\Delta x,\Delta y},x,y_{j+1}), S^x_{i+\frac{1}{2}}) + v\bar{\mathscr{R}}(\mathscr{D}_y(u_{\Delta x,\Delta y},x,y_j), S^x_{i+\frac{1}{2}}).\end{aligned}$$

Here $\mathscr{R}$ is the one-dimensional numerical integration operator, with the first argument as the integrand and the second the integration interval. The integral approximation can be written as a linear combination of the point values of the integrand, as described in [8], and the weights are determined by a WENO procedure. The operator $\bar{\mathscr{R}}$ approximates the integral as well and have the same arguments as $\mathscr{R}$. However, the weights in the representation of linear combinations are assumed to be linear.

Therefore the residual with $(2r-1)$th order accuracy can be represented by

$$\begin{aligned}\Phi_{i+\frac{1}{2},j+\frac{1}{2}} = {} & \sum_{k=-r+2}^{r-1} (a^k_{i+1,j} f(u_{i+1,j+k}) - a^k_{ij} f(u_{i,j+k})) \Delta y_{j+\frac{1}{2}} + \sum_{k=-r+2}^{r-1} (b^k_{i,j+1} g(u_{i+k,j+1}) - b^k_{ij} g(u_{i+k,j})) \Delta x_{i+\frac{1}{2}} \\ & - \mathscr{R}(\mathscr{R}\left(h(u_{\Delta x,\Delta y},x,y), S^y_{j+\frac{1}{2}}\right), S^x_{i+\frac{1}{2}}) - v \sum_{k=-r+2}^{r-1} (c^k \mathscr{D}_x(u_{\Delta x,\Delta y}, x_{i+1}, y_{j+k}) \\ & - c^k \mathscr{D}_x(u_{\Delta x,\Delta y}, x_i, y_{j+k})) \Delta y_{j+\frac{1}{2}} - v \sum_{k=-r+2}^{r-1} (d^k \mathscr{D}_y(u_{\Delta x,\Delta y}, x_{i+k}, y_{j+1}) \\ & - d^k \mathscr{D}_y(u_{\Delta x,\Delta y}, x_{i+k}, y_j)) \Delta x_{i+\frac{1}{2}}, \end{aligned} \tag{A.1}$$

where the coefficients $a^k_{ij} = a^k_{ij}(u_{i,j-r+2}, \ldots, u_{i,j+r-1})$ are Lipschitz continuous functions in all the arguments, and so are b^k_{ij}. For example, the WENO weights used in this paper are Lipschitz continuous since the smoothness indicators are smooth functions of u. Note that since we use linear weights in $\bar{\mathscr{R}}$ and we also assume uniform meshes for the proof of the Lax-Wendroff type theorem, the coefficients c^k and d^k are independent of (i,j).

In Eq. (A.1), the operators $\mathscr{D}_x$ and $\mathscr{D}_y$ are one-dimensional approximations of the first derivatives. By the fact that only uniform meshes and linear weights for the derivatives are considered, we have

$$\begin{aligned}\mathscr{D}_x(u_{\Delta x,\Delta y}, x_i, y) = {} & \sum_{m=-r+1}^{r-1} p^m u_{\Delta x,\Delta y}(x_{i+m}, y) \\ \mathscr{D}_y(u_{\Delta x,\Delta y}, x, y_j) = {} & \sum_{m=-r+1}^{r-1} q^m u_{\Delta x,\Delta y}(x, y_{j+m})\end{aligned} \tag{A.2}$$

with $(2r-2)$th order accuracy. Since we use symmetric linear weights to approximate the derivatives, and furthermore assume (in this proof) uniform meshes, we have

$$p^m = -p^{-m}, \quad q^m = -q^{-m}.$$

The distributed residuals, as defined in Section 3.1, are $\tilde{\Phi}^k_{i+\frac{1}{2},j+\frac{1}{2}}, k = 1,\ldots,4$, which are revised from the original one by adding a dissipation residual $\theta\Phi^k_{\text{diss}}$ defined in Eq. (3.6), where θ is the local discontinuity indicator. Suppose the residuals satisfy the conservation property, by the fact that $\sum_{k=1}^4 \Phi^k_{\text{diss}} = 0$

$$\Phi_{i+\frac{1}{2},j+\frac{1}{2}} = \sum_{k=1}^{4} \tilde{\Phi}^k_{i+\frac{1}{2},j+\frac{1}{2}} = \sum_{k=1}^{4} \Phi^k_{i+\frac{1}{2},j+\frac{1}{2}} \tag{A.3}$$

and residual property for the unrevised distributed residuals

$$\frac{|\Phi^k_{i+\frac{1}{2},j+\frac{1}{2}}|}{|\Phi_{i+\frac{1}{2},j+\frac{1}{2}}|} \leqslant C, \quad k = 1,\ldots,4. \tag{A.4}$$

Equipped with properties mentioned above, we have the following theorem.

Theorem A.1. *Assume that the flux function f and g in Eq. (3.1) are Lipschitz continuous, and the source term $h(u,x,y)$ is continuous in all arguments. Suppose that the mesh is uniform: $\Delta x_{i+\frac{1}{2}} = \Delta x$ and $\Delta y_{j+\frac{1}{2}} = \Delta y$ for all i,j. If $u_{\Delta x,\Delta y}$ is a steady state solution of Eq. (3.8) satisfying Eqs. (A.1), (A.3) and (A.4), and there is a function u with bounded total variation such that*

$$u_{\Delta x,\Delta y} \to u \quad \text{in } L^1(\mathbb{R}^2), \quad \text{as } \Delta x, \Delta y \to 0$$

and

$$\sup_{\Delta x,\Delta y} \sup_{x,y} |u_{\Delta x,\Delta y}(x,y)| \leqslant C$$

then u is a weak solution to Eq. (3.1).

Proof. Let $\varphi \in C_0^\infty(\mathbb{R}^2)$ be a test function, and denote $\varphi_{ij} = \varphi(x_i, y_j)$. At steady state, we have

$$\begin{aligned}
0 &= \sum_{i,j} (\tilde{\Phi}^1_{i-\frac{1}{2},j-\frac{1}{2}} + \tilde{\Phi}^2_{i-\frac{1}{2},j+\frac{1}{2}} + \tilde{\Phi}^3_{i+\frac{1}{2},j-\frac{1}{2}} + \tilde{\Phi}^4_{i+\frac{1}{2},j+\frac{1}{2}})\ \varphi_{ij} \\
&= \sum_{i,j} \Phi_{i-\frac{1}{2},j-\frac{1}{2}} \varphi_{ij} - \sum_{i,j} \Phi^2_{i-\frac{1}{2},j+\frac{1}{2}} (\varphi_{i,j+1} - \varphi_{ij}) - \sum_{i,j} \Phi^3_{i+\frac{1}{2},j-\frac{1}{2}} (\varphi_{i+1,j} - \varphi_{ij}) - \sum_{i,j} \Phi^4_{i+\frac{1}{2},j+\frac{1}{2}} (\varphi_{i+1,j+1} - \varphi_{ij}) + \delta\Delta^3 \\
&\quad \times \sum_{i,j} \left(\theta_{i-\frac{1}{2},j} \frac{u_{ij} - u_{i-1,j}}{\Delta x} + \theta_{i+\frac{1}{2},j} \frac{u_{ij} - u_{i+1,j}}{\Delta x} + \theta_{i,j-\frac{1}{2}} \frac{u_{ij} - u_{i,j-1}}{\Delta y} + \theta_{i,j+\frac{1}{2}} \frac{u_{ij} - u_{i,j+1}}{\Delta y} \right) \varphi_{ij} \\
&= \mathrm{I} + \mathrm{II} + \mathrm{III} + \mathrm{IV} + \mathrm{V}.
\end{aligned}$$

We look at the first summation term,

$$\begin{aligned}
\mathrm{I} &= \sum_{i,j} \Phi_{i-\frac{1}{2},j-\frac{1}{2}} \varphi_{ij} \\
&= \sum_{i,j} \sum_{k=-r+2}^{r-1} \left(a^k_{ij} f(u_{i,j+k}) - a^k_{i-1,j} f(u_{i-1,j+k}) \right) \Delta y\ \varphi_{i,j+1} + \sum_{i,j} \sum_{k=-r+2}^{r-1} \left(b^k_{ij} g(u_{i+k,j}) - b^k_{i,j-1} g(u_{i+k,j-1}) \right) \Delta x\ \varphi_{i+1,j} \\
&\quad - \sum_{i,j} \mathscr{R}(\mathscr{R}\left(h(u_{\Delta x,\Delta y}, x, y), S^y_{j-\frac{1}{2}}\right), S^x_{i-\frac{1}{2}})\ \varphi_{ij} - \sum_{i,j} \sum_{k=-r+2}^{r-1} (c^k \mathscr{D}_x(u_{\Delta x,\Delta y}, x_i, y_{j+k}) - c^k \mathscr{D}_x(u_{\Delta x,\Delta y}, x_{i-1}, y_{j+k})) \Delta y\ \varphi_{i,j+1} \\
&\quad - \sum_{i,j} \sum_{k=-r+2}^{r-1} (d^k \mathscr{D}_y(u_{\Delta x,\Delta y}, x_{i+k}, y_j) - d^k \mathscr{D}_y(u_{\Delta x,\Delta y}, x_{i+k}, y_{j-1})) \Delta x\ \varphi_{i+1,j} \\
&= -\sum_i \sum_j \mathscr{R}\left(f(u_{\Delta x,\Delta y}, x_i, y), S^y_{j+\frac{1}{2}}\right) \frac{\varphi_{i+1,j+1} - \varphi_{i,j+1}}{\Delta x} \Delta x - \sum_j \sum_i \mathscr{R}(g(u_{\Delta x,\Delta y}, x, y_j), S^x_{i+\frac{1}{2}}) \frac{\varphi_{i+1,j+1} - \varphi_{i+1,j}}{\Delta y} \Delta y \\
&\quad - \sum_{i,j} \mathscr{R}(\mathscr{R}\left(h(u_{\Delta x,\Delta y}, x, y), S^y_{j-\frac{1}{2}}\right), S^x_{i-\frac{1}{2}})\ \varphi_{ij} - \sum_{i,j} \sum_{k=-r+2}^{r-1} (c^k \mathscr{D}_x(u_{\Delta x,\Delta y}, x_i, y_{j+k}) - c^k \mathscr{D}_x(u_{\Delta x,\Delta y}, x_{i-1}, y_{j+k})) \Delta y\ \varphi_{i,j+1} \\
&\quad - \sum_{i,j} \sum_{k=-r+2}^{r-1} (d^k \mathscr{D}_y(u_{\Delta x,\Delta y}, x_{i+k}, y_j) - d^k \mathscr{D}_y(u_{\Delta x,\Delta y}, x_{i+k}, y_{j-1})) \Delta x\ \varphi_{i+1,j}
\end{aligned}$$

Note that

$$-\sum_i\sum_j \mathscr{R}\Big(f(u_{\Delta x,\Delta y},x_i,y),S^y_{j+\frac{1}{2}}\Big)\frac{\varphi_{i+1,j+1}-\varphi_{i,j+1}}{\Delta x}\Delta x \to -\int\int f(u)\ \varphi_x\,\mathrm{d}x\,\mathrm{d}y,\quad \text{as } \Delta x,\Delta y\to 0$$

$$-\sum_j\sum_i \mathscr{R}(g(u_{\Delta x,\Delta y},x,y_j),S^x_{i+\frac{1}{2}})\frac{\varphi_{i+1,j+1}-\varphi_{i+1,j}}{\Delta y}\Delta y \to -\int\int g(u)\ \varphi_y\,\mathrm{d}x\,\mathrm{d}y,\quad \text{as } \Delta x,\Delta y\to 0$$

and

$$-\sum_{i,j}\mathscr{R}(\mathscr{R}\Big(h(u_{\Delta x,\Delta y},x,y),S^y_{j-\frac{1}{2}}\Big),S^x_{i-\frac{1}{2}})\ \varphi_{ij}\to\int\int h(u,x,y)\ \varphi\,\mathrm{d}x\,\mathrm{d}y,\quad \text{as } \Delta x,\Delta y\to 0.$$

Moreover, by Eq. (A.2), we have

$$\begin{aligned}
&\sum_{i,j}\sum_{k=-r+2}^{r-1}(c^k\mathscr{D}_x(u_{\Delta x,\Delta y},x_i,y_{j+k})-c^k\mathscr{D}_x(u_{\Delta x,\Delta y},x_{i-1},y_{j+k}))\Delta y\ \varphi_{i,j+1}\\
&=\sum_{i,j}\sum_{k=-r+2}^{r-1}c^k\left(\sum_{m=-r+1}^{r-1}p^m u_{i+m.j+k}-\sum_{m=-r+1}^{r-1}p^m u_{i-1+m.j+k}\right)\Delta y\ \varphi_{i.j+1}\\
&=\sum_{i,j}\sum_{k=-r+2}^{r-1}\sum_{m=-r+1}^{r-1}c^k p^m(u_{i+m.j+k}-u_{i-1+m.j+k})\Delta y\ \varphi_{i,j+1}\\
&=-\sum_{i,j}\sum_{k=-r+2}^{r-1}\sum_{m=-r+1}^{r-1}c^k p^m u_{i+m,j+k}(\varphi_{i+1,j+1}-\varphi_{i,j+1})\Delta y\\
&=-\sum_{i,j}\sum_{k=-r+2}^{r-1}\sum_{m=-r+1}^{r-1}c^k p^m u_{i,j+k}(\varphi_{i+1-m,j+1}-\varphi_{i-m,j+1})\Delta y\\
&=\sum_{i,j}\sum_{k=-r+2}^{r-1}\sum_{m=-r+1}^{r-1}c^k p^m u_{i,j+k}(\varphi_{i+1+m,j+1}-\varphi_{i+m,j+1})\Delta y\\
&=\sum_{i,j}\mathscr{R}\Big(u_{\Delta x,\Delta y}(x_i,y),S^y_{j+\frac{1}{2}}\Big)\frac{\mathscr{D}_x(\varphi,x_{i+1},y_{j+1})-\mathscr{D}_x(\varphi,x_i,y_{j+1})}{\Delta x}\Delta x.
\end{aligned}$$

Note that as $\Delta x,\Delta y\to 0$,

$$\sum_{i,j}\mathscr{R}\Big(u_{\Delta x,\Delta y}(x_i,y),S^y_{j+\frac{1}{2}}\Big)\frac{\mathscr{D}_x(\varphi,x_{i+1},y_{j+1})-\mathscr{D}_x(\varphi,x_i,y_{j+1})}{\Delta x}\Delta x\to\int\int u\varphi_{xx}\,\mathrm{d}x\,\mathrm{d}y.$$

Therefore, as $\Delta x,\Delta y\to 0$,

$$\sum_{i,j}\sum_{k=-r+2}^{r-1}(c^k\mathscr{D}_x(u_{\Delta x,\Delta y},x_i,y_{j+k})-c^k\mathscr{D}_x(u_{\Delta x,\Delta y},x_{i-1},y_{j+k}))\Delta y\ \varphi_{i,j+1}\to\int\int u\varphi_{xx}\,\mathrm{d}x\,\mathrm{d}y. \tag{A.5}$$

Similarly,

$$\sum_{i,j}\sum_{k=-r+2}^{r-1}(d^k\mathscr{D}_y(u_{\Delta x,\Delta y},x_{i+k},y_j)-d^k\mathscr{D}_y(u_{\Delta x,\Delta y},x_{i+k},y_{j-1}))\Delta x\ \varphi_{i+1,j}\to\int\int u\varphi_{yy}\,\mathrm{d}x\,\mathrm{d}y. \tag{A.6}$$

So as $\Delta x,\Delta y\to 0$

$$\begin{aligned}
\mathrm{I}\to&-\int\int f(u)\ \varphi_x\,\mathrm{d}x\,\mathrm{d}y-\int\int g(u,x)\ \varphi_y\,\mathrm{d}x\,\mathrm{d}y-\int\int h(u,x,y)\ \varphi\,\mathrm{d}x\,\mathrm{d}y-\nu\int\int u\varphi_{xx}\,\mathrm{d}x\,\mathrm{d}y\\
&-\nu\int\int u\varphi_{yy}\,\mathrm{d}x\,\mathrm{d}y.
\end{aligned}$$

Next, we estimate the second term II

$$
\begin{aligned}
|\mathrm{II}| &= \left|\sum_{i,j} \Phi^2_{i-\frac{1}{2},j+\frac{1}{2}}(\varphi_{i,j+1}-\varphi_{ij})\right| \leqslant \sum_{i,j} |\Phi^2_{i-\frac{1}{2},j+\frac{1}{2}}||\varphi_{i,j+1}-\varphi_{ij}| \leqslant C\sum_{i,j} |\Phi_{i-\frac{1}{2},j+\frac{1}{2}}||\varphi_{i,j+1}-\varphi_{ij}| \\
&\leqslant C\sum_{i,j}\sum_{k=-r+2}^{r-1} |a^k_{ij}f(u_{i,j+k}) - a^k_{i-1,j}f(u_{i-1,j+k})||\varphi_{i,j+1}-\varphi_{ij}|\Delta y + C\sum_{i,j}\sum_{k=-r+2}^{r-1} |b^k_{i,j+1}g(u_{i+k,j+1}) \\
&\quad - b^k_{ij}g(u_{i+k,j})||\varphi_{i,j+1}-\varphi_{ij}|\Delta x + C\sum_{i,j} \mathscr{R}(\mathscr{R}\left(|h(u_{\Delta x,\Delta y},x,y)|, S^y_{j+\frac{1}{2}}\right), S^x_{i-\frac{1}{2}})\ |\varphi_{i,j+1}-\varphi_{i,j}| \\
&\quad + C\sum_{i,j}\sum_{k=-r+2}^{r-1} |c^k\mathscr{D}_x(u_{\Delta x,\Delta y},x_i,y_{j+k}) - c^k\mathscr{D}_x(u_{\Delta x,\Delta y},x_{i-1},y_{j+k})||\varphi_{i,j+1}-\varphi_{i,j}|\Delta y \\
&\quad + C\sum_{i,j}\sum_{k=-r+2}^{r-1} |d^k\mathscr{D}_y(u_{\Delta x,\Delta y},x_{i+k},y_{j+1}) - d^k\mathscr{D}_y(u_{\Delta x,\Delta y},x_{i+k},y_j)||\varphi_{i,j+1}-\varphi_{i,j}|\Delta x.
\end{aligned}
$$

Since $\int\int |h(u,x,y)||\varphi_y|\,\mathrm{d}x\,\mathrm{d}y$ is bounded, with Lipschitz continuity of a^k_{ij}, b^k_{ij} and the flux functions, boundedness of u_{ij}, (A.2) and $0 < C_1 \leqslant |\Delta x/\Delta y| \leqslant C_2$, we have

$$
|\mathrm{II}| \leqslant C_3\sum_{i,j} |u_{i,j}-u_{i-1,j}|\Delta x\Delta y + C_3\sum_{i,j} |u_{i,j}-u_{i,j-1}|\Delta x\Delta y + \mathrm{O}(\Delta y). \tag{A.7}
$$

The first term on the right side of (A.7) can be estimated by

$$
\begin{aligned}
\sum_{i,j} |u_{i,j}-u_{i-1,j}|\Delta x\Delta y &\leqslant \sum_{i,j} |u_{ij}-u(x_i,y_j)|\Delta x\Delta y + \Delta y\sum_i\sum_j |u(x_i,y_j)-u(x_{i-1},y_j)|\Delta x + \sum_{i,j} |u(x_{i-1},y_j) \\
&\quad - u_{i-1,j}|\Delta x\Delta y
\end{aligned}
$$

and it goes to zero when the mesh is refined due to the L^1 convergence of the numerical solution and the fact that the limit solution u has bounded total variation. Similarly, the second term on the right side of (A.7) also goes to zero when the mesh is refined. Therefore, II $\to 0$ as $\Delta x,\Delta y \to 0$. Similarly, we can easily prove that III, IV $\to 0$ as $\Delta x,\Delta y \to 0$.

Lastly,

$$
\begin{aligned}
\mathrm{V} &= \delta\Delta^3\sum_{i,j}\left(\theta_{i-\frac{1}{2},j}\frac{u_{ij}-u_{i-1,j}}{\Delta x} - \theta_{i+\frac{1}{2},j}\frac{u_{i+1,j}-u_{ij}}{\Delta x}\right)\varphi_{ij} + \delta\Delta^3\sum_{i,j}\left(\theta_{i,j-\frac{1}{2}}\frac{u_{ij}-u_{i,j-1}}{\Delta y} - \theta_{i,j+\frac{1}{2}}\frac{u_{i,j+1}-u_{ij}}{\Delta y}\right)\varphi_{ij} \\
&= \delta\Delta^3\sum_{i,j}\theta_{i-\frac{1}{2},j}(u_{ij}-u_{i-1,j})\frac{\varphi_{ij}-\varphi_{i-1,j}}{\Delta x} + \delta\Delta^3\sum_{i,j}\theta_{i,j-\frac{1}{2}}(u_{ij}-u_{i,j-1})\frac{\varphi_{ij}-\varphi_{i,j-1}}{\Delta y}.
\end{aligned}
$$

Clearly, the boundedness of θ and u_{ij} implies that $|\mathrm{V}|$ is bounded by $\mathrm{O}(\Delta)$, hence $\mathrm{V} \to 0$ as $\Delta \to 0$. We can now conclude that

$$
-\int\int f(u)\varphi_x\,\mathrm{d}x\,\mathrm{d}y - \int\int g(u)\varphi_y\,\mathrm{d}x\,\mathrm{d}y = \int\int h(u,x,y)\varphi\,\mathrm{d}x\,\mathrm{d}y + \nu\int\int u\varphi_{xx}\,\mathrm{d}x\,\mathrm{d}y + \nu\int\int u\varphi_{yy}\,\mathrm{d}x\,\mathrm{d}y
$$

so u is a weak solution of Eq. (3.1). □

References

[1] R. Abgrall, Toward the ultimate conservative scheme: following the quest, Journal of Computational Physics 167 (2001) 277–315.

[2] R. Abgrall, Essentially non oscillatory residual distribution schemes for hyperbolic problems, Journal of Computational Physics 214 (2006) 773–808.

[3] R. Abgrall, T. Barth, Residual distribution schemes for conservation laws via adaptive quadrature, SIAM Journal of Scientific Computing 24 (2002) 732–769.

[4] R. Abgrall, K. Mer, B. Nkonga, A Lax-Wendroff type theorem for residual schemes, in: M. Hafez, J.J. Chattot (Eds.), Innovative Methods for Numerical Solutions of Partial Differential Equations, World Scientific, Singapore, 2002, pp. 243–266.
[5] R. Abgrall, M. Mezine, Construction of second order accurate monotone and stable residual distribution schemes for steady problems, Journal of Computational Physics 195 (2004) 474–507.
[6] R. Abgrall, P.L. Roe, High order fluctuation scheme on triangular meshes, Journal of Scientific Computing 19 (2003) 3–36.
[7] D. Caraeni, L. Fuchs, Compact third-order multidimensional upwind scheme for Navier–Stokes simulations, Theoretical and Computational Fluid Dynamics 15 (2002) 373–401.
[8] C.-S. Chou, C.-W. Shu High order residual distribution conservative finite difference WENO schemes for steady state problems on non-smooth meshes, Journal of Computational Physics 214 (2006) 698–724.
[9] H. Deconinck, R. Struijs, G. Bourgeois, P. Roe, Compact advection schemes on unstructured meshes, Computational Fluid Dynamics (1993), VKI Lecture Series 1993-04.
[10] A. Harten, High resolution schemes for hyperbolic conservation laws, Journal of Computational Physics 49 (1983) 357–393.
[11] J. Jerome, C.-W. Shu, Energy models for one-carrier transport in semiconductor devices, in: W. Coughran, J. Cole, P. Lloyd, J. White (Eds.), IMA Volumes in Mathematics and Its Applications, vol. 59, Springer-Verlag, Berlin, 1994, pp. 185–207.
[12] G. Jiang, C.-W. Shu, Efficient implementation of weighted ENO schemes, Journal of Computational Physics 126 (1996) 202–228.
[13] A. Lerat, C. Corre, A residual-based compact scheme for the compressible Navier–Stokes equations, Journal of Computational Physics 170 (2001) 642–675.
[14] F. Marpeau, R. Abgrall, Residual distribution schemes on quadrilateral meshes, Journal of Scientific Computing. Published online with DOI: 10.1007/s10915-005-9023-2.
[15] H. Nishikawa, Higher order discretization of diffusion terms in residual distribution methods, Computational Fluid Dynamics (2005), VKI Lecture Series 2005-01.
[16] H. Nishikawa, P.L. Roe, On high order fluctuation splitting schemes for Navier–Stokes equations, in: Third International Conference on Computational Fluid Dynamics, Toronto, CA, 2004.
[17] H. Paillère, J. Boxho, G. Degrez, H. Deconinck, Multidimensional upwind residual distribution schemes for the convection–diffusion equation, International Journal for Numerical Methods in Fluids 23 (1996) 923–936.
[18] M. Ricchiuto, N. Villedieu, R. Abgrall, H. Deconinck, Higher order residual distribution schemes: discontinuity capturing crosswind dissipation and extension to advection–diffusion, Computational Fluid Dynamics (2005), VKI Lecture Series 2005-01.
[19] P.L. Roe, Approximate Riemann solvers, parameter vectors, and difference schemes, Journal of Computational Physics 43 (1981) 357–372.
[20] P.L. Roe, D. Sidilkover, Optimum positive linear schemes for advection in two or three dimensions, SIAM Journal of Numerical Analysis 29 (1992) 1542–1588.
[21] C.-W. Shu, S. Osher, Efficient implementation of essentially non-oscillatory shock-capturing schemes, Journal of Computational Physics 77 (1988) 439–471.
[22] R. Struijs, H. Deconinck, P.L. Roe, Fluctuation splitting schemes for the 2D Euler equations, Computational Fluid Dynamics (1991), VKI Lecture Series 1991-01.
[23] E. van der Weide, H. Deconinck, Fluctuation splitting schemes for the Euler equations on quadrilateral grids, in: Numerical Methods for Fluid Dynamics V, Oxford University Press, Oxford, UK, 1995, pp. 623–630.
[24] E. van der Weide, H. Deconinck, Positive matrix distribution schemes for hyperbolic systems, in: Dèsidèri, C. Hirch, P. Le Tallec, M. Pandolfi, J. Pèriaux (Eds.), Computational Fluid Dynamics, Wiley, New York, 1996, pp. 747–753.
[25] E. van der Weide, H. Deconinck, G. Degrez, A parallel, implicit, multi-dimensional upwind, residual distribution method for the Navier–Stokes equations on unstructured grids, Computational Mechanics 23 (1999) 199–208.
[26] Z. Xu, C.-W. Shu, Anti-diffusive flux corrections for high order finite difference WENO schemes, Journal of Computational Physics 205 (2005) 458–485.